DRA/HQ.

aer

(NASA-CR-174146) OUTER SATELLITE ATMOSPHERES: THEIR NATURE AND PLANETARY INTERACTIONS Annual Report, 1 Jun. 1983 - 31 Jul. 1984 (Atmospheric and Environmental Research) 56 p EC AC4/MF AC1 CSCL 03B G3/91

N85-13759

Unclas 24524

ATMOSPHERIC AND ENVIRONMENTAL RESEARCH, INC.
CAMBRIDGE, MASSACHUSETTS

OUTER SATELLITE ATMOSPHERES: THEIR NATURE AND PLANETARY INTERACTIONS

Annual Report for Period
June 1, 1983 to July 31, 1984

Prepared for

NASA Headquarters
Washington, DC 20546

Prepared by

William H. Smyth
and
Michael R. Combi

Atmospheric and Environmental Research, Inc.
840 Memorial Drive
Cambridge, Massachusetts 02139

TECHNICAL REPORT STANDARD TITLE PAGE

1. Report No.	2. Government Accession No	3. Recipient's Catalog No.

4. Title and Subtitle	5. Report Date
Outer Satellite Atmospheres: Their Nature and Planetary Interactions	November 1984
	6. Performing Organization Code
7. Author(s) William H. Smyth and Michael R. Combi	8. Performing Organization Report No
9. Performing Organization Name and Address Atmospheric and Environmental Research, Inc. 840 Memorial Drive Cambridge, MA 02139	10. Work Unit No.
	11. Contract or Grant No. NASW-3387
	13. Type of Report and Period Covered Annual Report June 1, 1983 - July 31, 1984
12. Sponsoring Agency Name and Address NASA Headquarters Headquarters Contract Division Washington, DC 20546	14. Sponsoring Agency Code HWC-2
15. Supplementary Notes	

16. Abstract

Significant insights regarding the nature and interactions of Io and the planetary magnetosphere have been gained through modeling studies of the spatial morphology and brightness of the Io sodium cloud. East-west intensity asymmetries in Region A are consistent with an east-west electric field and the offset of the magnetic and planetary-spin axes. East-west orbital asymmetries and the absolute brightness of Region B suggest a low-velocity ($\sim$3 km sec^{-1}) satellite source of $\sim$1-2 x 10^{26} sodium atoms sec^{-1}. The time-varying spatial structure of the sodium directional features in near Region C provides direct evidence for a magnetospheric-wind-driven escape mechanism with a high-velocity ($\sim$20 km sec^{-1}) source of $\sim$1 x 10^{26} atoms sec^{-1} and a flux distribution enhanced at the equator relative to the poles. A model for the Io potassium cloud is presented and analysis of data suggests a low-velocity source rate of $\sim$5 x 10^{24} atoms sec^{-1}. To understand the role of Titan and non-Titan sources for H atoms in the Saturn system, the lifetime of hydrogen in the planetosphere magnetosphere has been incorporated into the earlier Titan torus model of Smyth (1981) and its expected impact discussed. A particle trajectory model for cometary hydrogen is presented and applied to the Lyman-α distribution of Comet Kohoutek (1973XII).

17. Key Words (Selected by Author(s))	18. Distribution Statement
satellite atmospheres planetary magnetospheres comets	

19. Security Classif. (of this report)	20. Security Classif. (of this page)	21. No. of Pages	22. Price*
Unclassified	Unclassified		

*For sale by the Clearinghouse for Federal Scientific and Technical Information, Springfield, Virginia 22151.

TABLE OF CONTENTS

LIST OF FIGURES

LIST OF TABLES

I. INTRODUCTION

The progress achieved in the third year of this three-year research program is reported. The overall research program is organized into three different subjects: (1) the Jupiter system, (2) the Saturn system, and (3) Comets. In the Jupiter system, the extended atmospheres of Io and their relations and interactions with the planetary magnetosphere are the topic of interest. In the Saturn system, the hydrogen torus of Titan, the atmospheres associated with the planetary rings, and the extended atmospheres of the E-ring icy satellites as well as the planet are the topics of concern. For comets, the dust and gas clouds in the inner and outer coma are the areas of focus.

The three primary goals of the overall program are (1) to better understand the characteristics of the local atmosphere of Io and the manner in which it interacts and delivers a significant source of heavy-ion plasma to the planetary magnetosphere, (2) to understand the spatial distribution of hydrogen in the Saturn system in terms of the planet, its rings and its satellites, and to better define the source of protons for the magnetosphere, and (3) to provide fresh insight into the chemical and physical nature of comets through study of their extended atmospheres. These research objectives are important in achieving better understanding of the basic satellite and magnetospheric processes in the outer solar system and basic comet and solar radiation processes in the inner solar system. To pursue these goals, the research program has employed both exploratory calculations (to uncover important physical mechanisms) and more-refined model calculations to evaluate the quantitative significance of these mechanisms.

For the Jupiter system, the overall three-year research plan is summarized in Table 1. There are three major subjects. The first subject, the Io sodium cloud, is divided into five subtopics. Efforts during the third year have been focused upon subtopics (i), (iii) and (iv). Efforts originally to be applied to subtopic (ii) were reassigned to topic (iv) where the same objective was able to be pursued more effectively using the more recently discovered directional feature data of Pilcher (1982). For the Io potassium cloud, the second topic in Table 1, model development was completed this year and applied to observational data of Trafton (1981). The third topic of Table 1 has remained inactive, since no new gas clouds were discovered during the

Table 1

JUPITER SYSTEM: THREE-YEAR PLAN FOR MODEL DEVELOPMENT AND ANALYSIS

Subject	First Year	Second Year	Third Year
Io Sodium Cloud Model Development	Update the model to include the oscillating Io plasma torus as an ionization sink (Phase 1) and simultaneously include the effects of solar radiation pressure (Phase 2)	Enhance CPU execution efficiency of the numerical model	-
(i) 2-D Intensity Morphology	-	Perform initial model calculations and compare with observed images of Murcray (1978) to determine the sodium atom flux and insight into the cloud structure	Perform model calculations to analyze the East-West asymmetries and the North-South alternating asymmetry of the cloud
(ii) Line Profiles	-	-	Perform model calculations for measured line profiles to study the satellite emission mechanism
(iii) Io Plasma Torus Interactions	Adopt a description of the electron density and temperature in the plasma torus and calculate the sodium electron impact ionization lifetime	Evaluate the effects of elastic ion-sodium collisions	Improve description of electron plasma data
(iv) Directional Features	Perform very preliminary one-orbit modeling analysis to roughly characterize the emission velocity of the features	Enhance model and analysis procedure. Perform initial model calculations to study the data of Pilcher (1982)	Perform additional model calculations to further refine insights into the emission mechanism
Io Potassium Cloud	Calculate the potassium electron impact ionization lifetime in the plasma torus. Obtain the solar spectrum for the two K emission intensity and acceleration produced by solar resonance scattering	Initiate development of the potassium cloud model by suitably modifying the sodium cloud model	Complete model development and perform model calculations appropriate to the observations of Trafton (1981)
Other Io Clouds	-	-	Provide exploratory modeling for newly discovered gas clouds

third year. Progress achieved in the first two subjects of Table 1 is discussed in section II.

For the Saturn system, the overall three year research plan is summarized in Table 2 and is organized into the study of four objects, each known or expected to provide a source of hydrogen atoms and ultimately protons to the circumplanetary space. During the third year, major emphasis has been placed upon better understanding the role of Titan (and hence ultimately non-Titan sources) in the new light that the planet may itself also provide a significant source of hydrogen to the Saturn system (Shemansky and Smith, 1982). Progress resulting from these efforts is discussed in Section III.

For comets, our research efforts have been reactivated in the third year as scheduled in Table 2. The AER particle trajectory model has been further developed and applied to the extended hydrogen atmospheres of comets. Results of these efforts are reported in section IV.

Table 2

SATURN SYSTEM AND COMETS: THREE-YEAR PLAN FOR MODEL DEVELOPMENT AND ANALYSIS

Extended Atmosphere	First Year	Second Year	Third Year
Saturn System Planet	–	New Idea: The planet may be a source of H for the Saturn system (Shemansky and Smith, 1982) and may provide an alternate explanation for the ring atmosphere and part of the Titan H torus cloud	Further evaluate Saturn as an H source and, if warranted, develop a model for an extended H atmosphere for the planet
Saturn's Rings	Perform preliminary study for photo-sputtering of H_2O ring-ice as an H source (problem too much oxygen remaining near rings)	–	Assess the importance of the rings as a source of gas for the Saturn system
E-Ring Satellites	–	Perform limited studies to ascertain the physical domain of H atoms for E-ring satellite sources	Assess the importance of the satellites as a source of gas for the Saturn system
Titan	–	Examine post-Voyager data for H atoms in the Saturn system Update pre-Voyager model to include a spatially dependent ionization of H in the Saturn magnetosphere	Complete the update of the Titan H torus model Perform model calculations and compare to the Voyager UVS data to ascertain the role of Titan as a source of H atoms
Comets	–	–	Complete model refinements Apply model to comet coma observations

II. THE JUPITER SYSTEM

2.1 Introduction

The three-year research plans for the Io sodium cloud and Io potassium cloud are summarized in Table 1. Studies for the Io sodium cloud are subdivided into a general model development and four separate subtopics organized around the different types of observational data that are available. Progress in the third year has been built upon our primary model-development activities of the first year and the initial phase of model application undertaken during the second year. The improved models, which now include the oscillating Io plasma torus as a time-space varying sink for sodium and potassium as well as even more complex space-time dependences, provide new and powerful modeling tools that have allowed us to draw some significant conclusions from observational data. These conclusions are discussed below.

2.2 Interactions of the Io Sodium Cloud and Plasma Torus

The space-time history of an ensemble of sodium cloud atoms initially ejected from Io and moving through the inner magnetosphere of Jupiter depends upon the physical processes by which these atoms may interact with the plasma torus. There are four basic processes: electron impact ionization, charge exchange reactions, photoionization, and elastic ion-neutral collisions. As discussed below, ionization by electrons appears to be by far the dominant process for shaping the spatial morphology of the sodium cloud in Region B and in near Region C.

The first three of the plasma-atom interactions noted above effectively remove sodium from the cloud and hence determine its lifetime in the plasma torus. Ionization of sodium by electron impact ionization is very rapid in the plasma torus ($\gtrsim$ 1 hour lifetime based upon Voyager 1 plasma data; see Figure 1). Charge exchange reactions remove neutral sodium from the cloud and create in its place either an ion (e.g., $X^{++} + Na \rightarrow X^{+} + Na^{+}$) or a fast neutral (~60 km sec^{-1}, which was the corotating ion X^{+} before the reaction $X^{+} + Na \rightarrow X^{+} + Na^{+}$). The fast neutral so produced rapidly escapes from the Jupiter system unless it is trapped in the outer magnetosphere. For the case of resonance charge exchange ($X^{+} = Na^{+}$), the fast neutral is sodium, but it moves so rapidly that it appears to contribute minimally to the bright Region B and close Region C portion of the cloud, although it may be a very important

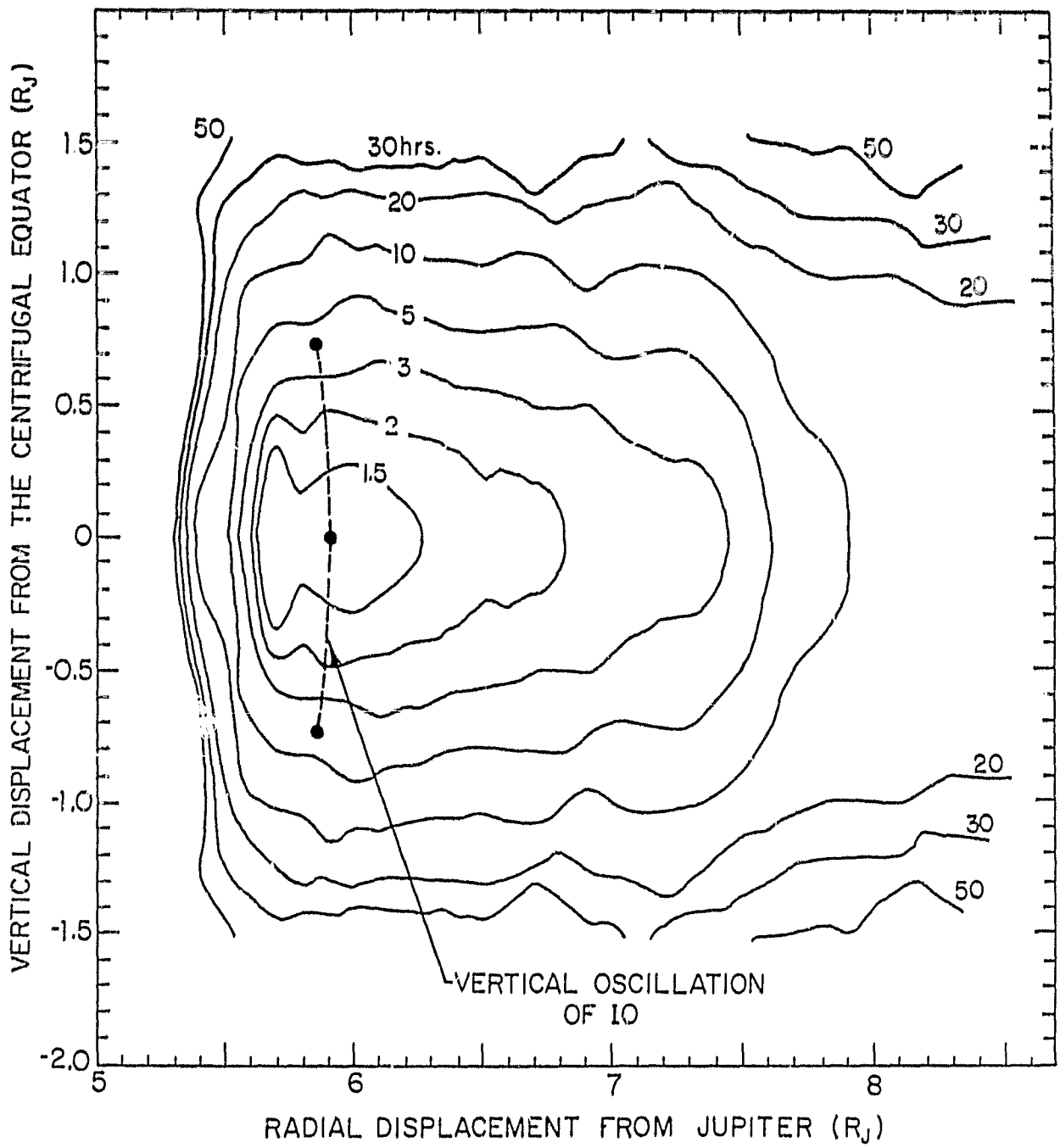

Figure 1. Sodium Electron Impact Ionization Lifetime in the Io Plasma Torus.

The lifetime calculation from Smyth (1983) is based upon the cross-section measured by McFarland (1965), McFarland and Kinney (1965), and Zapesochnyi and Aleksakhin (1968), Voyager 1 *in situ* measurements of the plasma density (Bridge, Sullivan and Bagenal, 1980; Bagenal and Sullivan, 1981), and Voyager 1 UVS (Shemansky, 1980) and *in situ* measurements (Scudder, Sittler and Bridge, 1981) for the electron temperature. The two-dimensional common temperature model of Bagenal and Sullivan (1981) was selected to describe the electron density.

source for the fast component of the fainter remote-sodium observed by Brown and Schneider (1981) and more recently near Io by Schneider, Hunten and Brown (1984) and Trauger (1984). Charge exchange reactions for Region B and close Region C may therefore be treated simply as a lifetime process. Based upon the best Voyager 1 data (Bagenal 1984; Shemansky, 1984) and available cross-sections (Johnson and Strobel, 1982), the charge exchange lifetime for sodium in the plasma torus is dominated, by more than an order of magnitude, by electron impact ionization for radial distances beyond about 5.5 R_J (where the electron temperature $\gtrsim$ 4 ev), and hence charge exchange becomes ineffective. Inside of about 5.5 R_J, the electron and ion temperatures become cool, the electron impact ionization lifetime becomes consequently larger (see Figure 1) and the plasma torus collapses latitudinally to within about 0.2 R_J of the plasma symmetry plane. The lifetimes for resonance charge exchange and for non-resonance charge exchange (only O^{++}, S^{++} and S^{+++} have significant cross-sections with Na) therefore eventually compete and become more important than electron impact ionization inside of 5.5 R_J. At that point, however, the ions are confined so closely to the centrifugal symmetry plane of the plasma torus and have sufficiently large lifetimes that they are incapable of having any significant spatial overlap and effect during the nominal 20 hours of flight time of sodium atoms in the forward cloud (see Figure 2). Even less important is the photoionization lifetime for sodium atoms near Jupiter. It is about 400 hours and is only important as a sodium sink far outside of the plasma torus.

Elastic collisions between plasma torus heavy ions and atoms of the sodium cloud may also occur. As noted by Brown, Pilcher and Strobel (1983), "hard" ion-sodium atom collisions (resulting from the repulsive core of the interatomic potential) cause a simple loss of material from the Io-connected cloud and are, in this way, similar to the resonance charge exchange reaction discussed above. "Soft" ion-sodium atom collisions (resulting from the attractive force produced by the dipole moment induced by the passing ionic charge) will result in much smaller momentum transfer that may sever the kinematic connection between the initial escape conditions at Io and the morphological structure of the near (Region B, close Region C) cloud. This effect of soft collisions, if important, could then greatly complicate the simpler model description adopted here. To estimate the importance of these soft collisions, Brown, Pilcher and Strobel (1983) used the momentum transfer

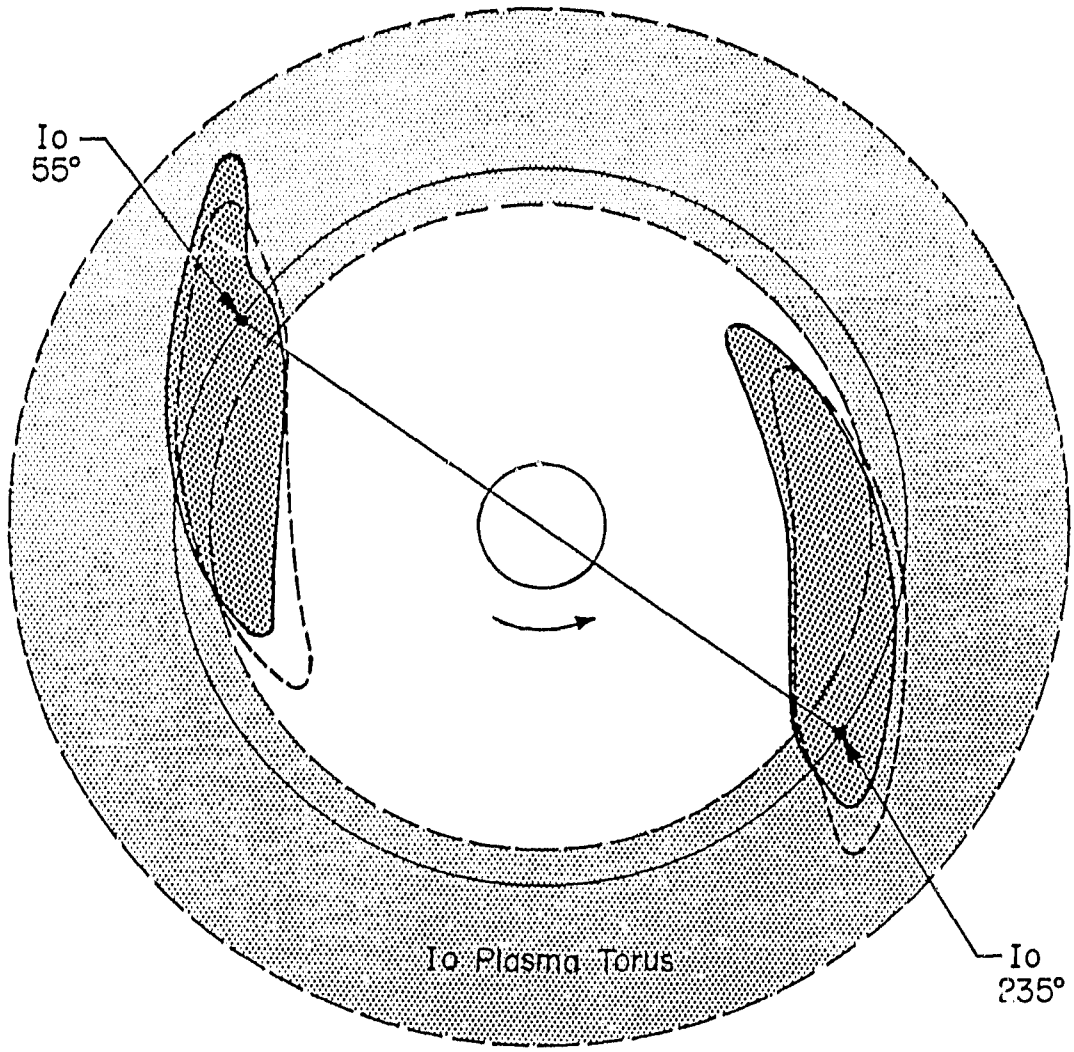

Figure 2. Interaction of the Sodium Cloud and the Plasma Torus. The spatially projected overlap in the satellite plane of the Io plasma torus with the solar radiation perturbed cloud shape (solid boundary with heavy shading) and with the unperturbed cloud shape (heavy dashed boundary) is indicated for the diametrically opposite satellite phase angles. The cloud shape illustrates the envelope of sodium atoms after 20 hours of flight time.

cross-section based upon the ion-atom polarization potential. For the large polarizability of sodium, however, this potential provides only an overestimation of the strength of the interaction (Johnson, 1984). This occurs because the correct potential for sodium at the values of the impact parameters of interest is actually a combination of a comparable repulsive potential and attractive polarization potential which partially cancel and reduce the value of the true potential and hence its cross-section. The true potential for sodium is not presently available. Adopting this polarization cross-section to establish an upper bound, the soft elastic collision time for sodium is evaluated in the plasma torus for Voyager 1 plasma conditions and shown in Figure 3. The collision time is more than an order of magnitude larger than the electron impact ionization lifetime for sodium beyond about 5.5 R_J. For the Region B overlap beyond about 5.5 R_J, the average collision time is no smaller than 50 to 100 hours in the oscillating torus. Since it takes a nominal 5 hours for the fraction of the sodium atoms which survive ionization by electrons to exit inside of the plasma torus, this 50 to 100 hour lifetime implies that 5-10% of these surviving sodium atoms will suffer a soft elastic collision. Since this is an overestimation, the real effect based upon a true potential for sodium must then be at best only a few percent. Inside of 5.5 R_J, the situation is even less promising, because the ions are confined so closely to the centrifugal symmetry plane of the plasma torus that they are incapable of having any significant overlap and effect during the remaining nominal 15 hours of flight time of sodium atoms in the forward cloud (see Figure 2).

2.3 The Io Sodium Cloud: Region A

The east-west intensity asymmetry of Region A, discovered and documented by Bergstralh et al. (1975 and 1977), was recently attributed by Smyth (1983) to the effects of both solar radiation pressure (for very low velocity escape of sodium from Io) and the plasma torus sink (for higher velocity escape of sodium from Io). The need, noted by Smyth (1983), to further clarify the role played by the Io plasma torus sink, has been initially addressed this past year. This has been accomplished by using our new Io sodium cloud model, which explicitly includes the oscillating plasma torus sink, to calculate the brightness of Region A as viewed through the rectangular viewing slit adopted by Bergstralh et al. (1975, 1977). The effects of the oscillating plasma

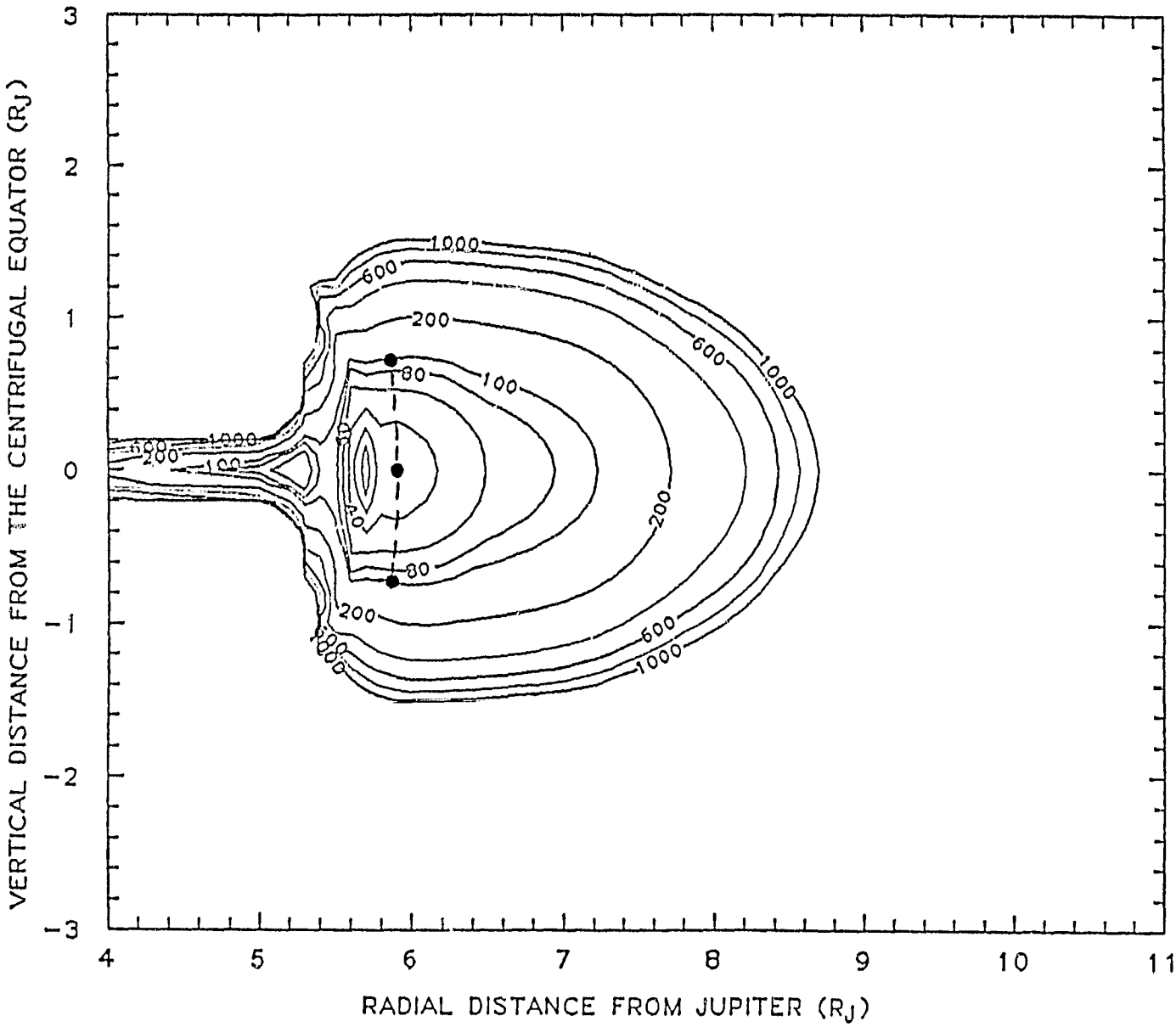

Figure 3. Elastic Collision Lifetime of Sodium Atoms in the Io Plasma Torus. The lifetime (in hours) is based upon the polarization lifetime of Brown, Pilcher and Strobel (1983) and Voyager 1 plasma torus conditions (Bagenal, 1984; Shemansky, 1984). The smallest collision lifetime of about 20 hours occurs on the centrifugal equator at a radial distance from Jupiter of 5.7 R_J, around which unlabeled lifetime contours of 25 and 30 hours are shown. The motion of Io (at 5.9 R_J) resulting from the oscillation of the plasma torus about the satelliite orbit plane is also indicated.

torus sink, the presence of an east-west electric field in the magnetosphere (Ip and Goertz, 1983; Barbosa and Kivelson, 1983), and the impact of the offset dipole nature of the planetary magnetic field (Acuña, Behannon, and Connerney, 1983) have been preliminarily assessed and are briefly discussed here.

The oscillation of the plasma torus about the satellite plane introduces a modulation in the brightness of Region A because of the varying sodium lifetime at Io, but it does not introduce any east-west intensity asymmetry (if the plasma properties are independent of system III magnetic longitude). An east-west electric field in the magnetosphere has recently been proposed by Ip and Goertz (1983) and Barbosa and Kivelson (1983) to explain the dawn-dusk asymmetry in the torus ion emission brightness measured by the Voyager UVS instrument (Sandel and Broadfoot, 1982; Shemansky and Sandel, 1982). Their proposed electric field essentially shifts the plasma torus to a new center that is displaced toward the east by about 0.18 to 0.20 Jupiter radii. For a given radial displacement from Jupiter, this provides an overall relative east to west shift of the plasma torus properties by twice this amount and gives rise to a significant east-west asymmetry in the sodium sink because of the sharp temperature gradient inside of Io's orbit. This asymmetry in the sodium sink is graphically illustrated by comparison of electron impact ionization of sodium at Io's orbital position in Figure 4 (with no electric field) and Figure 5 (with an electric field producing a nominal shift of 0.15 R_J). This east-west asymmetry in the sink provides an east-west intensity asymmetry in the brightness of Region A that is in agreement with the value observed by Bergstralh et al. (1975, 1977). This agreement is shown in Figure 6, where model calculations incorporating different values of the shift parameter are compared with the observations. Inclusion in the model calculations of a 0.12 R_J offset of the dipole magnetic field toward 149° System III longitude, in addition to the east-west electric field, produces the plasma sink illustrated in Figure 7. This additional offset modulates the east-west intensity about the mean value established by the east-west electric field as illustrated in Figure 6. This modulation may account for some of the apparent scatter present in the intensity data of Bergstralh et al. (1975, 1977).

Figure 4

ELECTRON IMPACT IONIZATION LIFETIMES OF SODIUM AT IO'S POSITION

for a

Plasma Torus Centered on Jupiter

(hours)

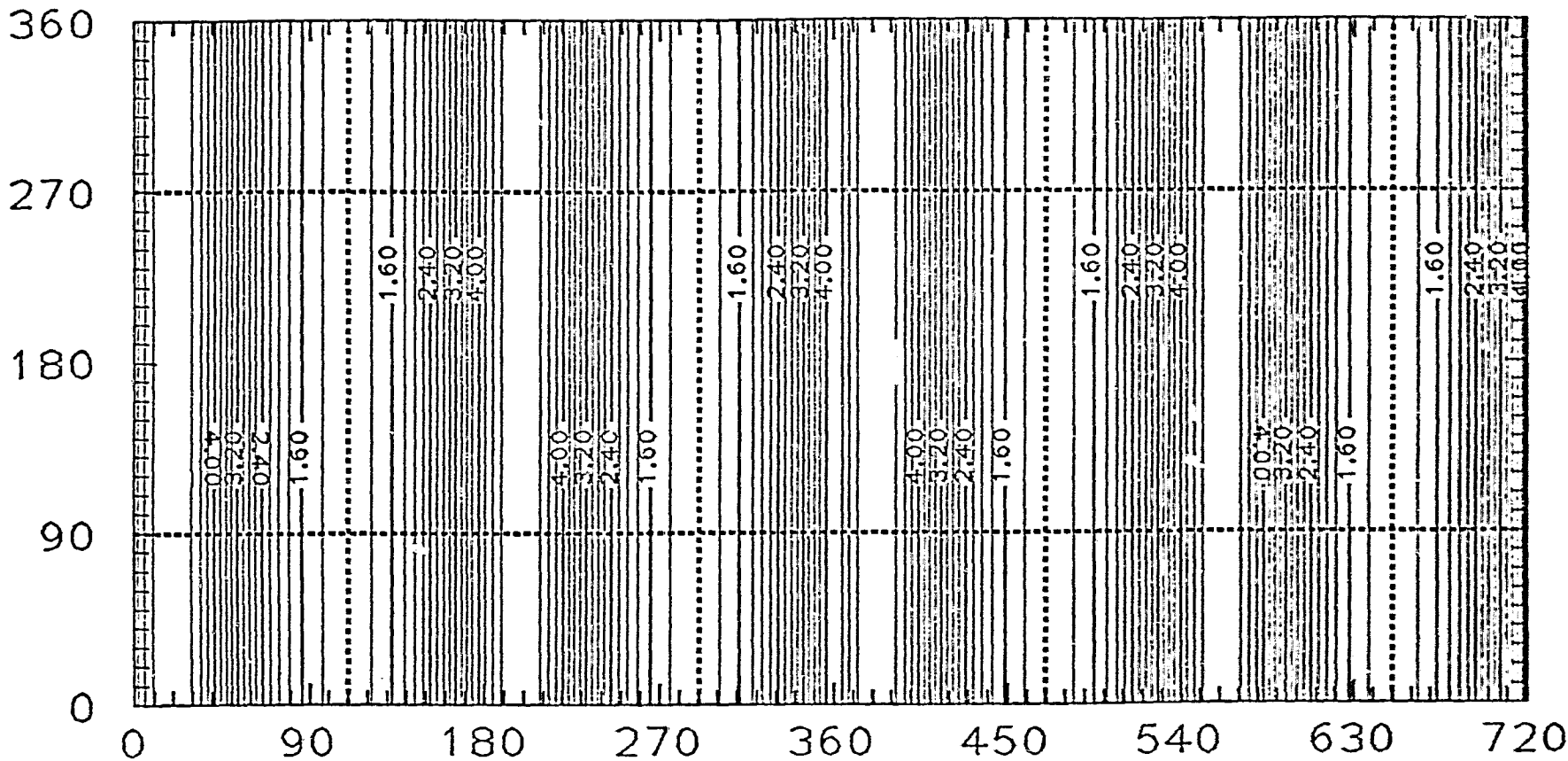

Figure 5

ELECTRON IMPACT IONIZATION LIFETIMES OF SODIUM AT IO'S POSITION

for an
East-West Electric Field
(hours)

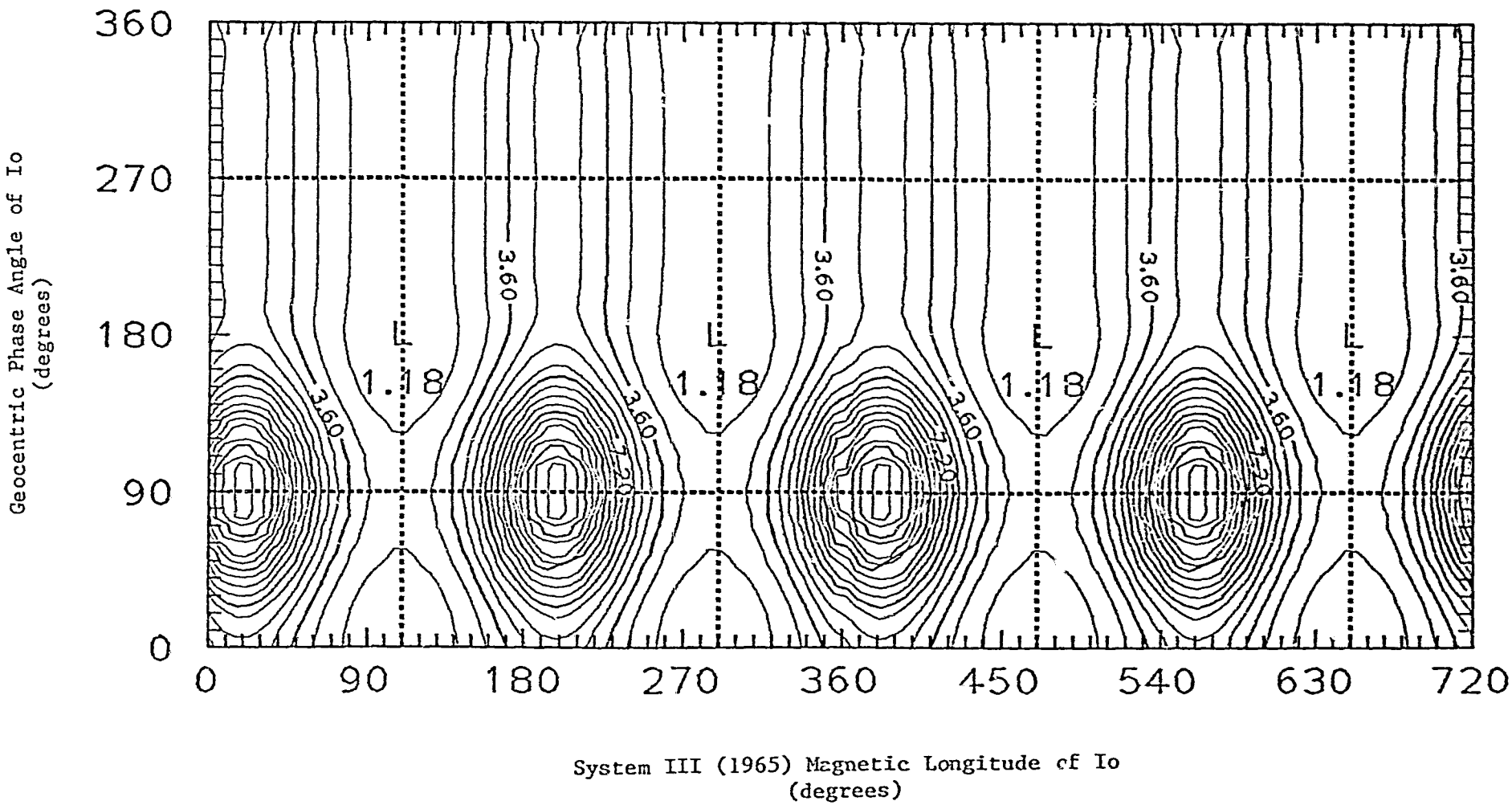

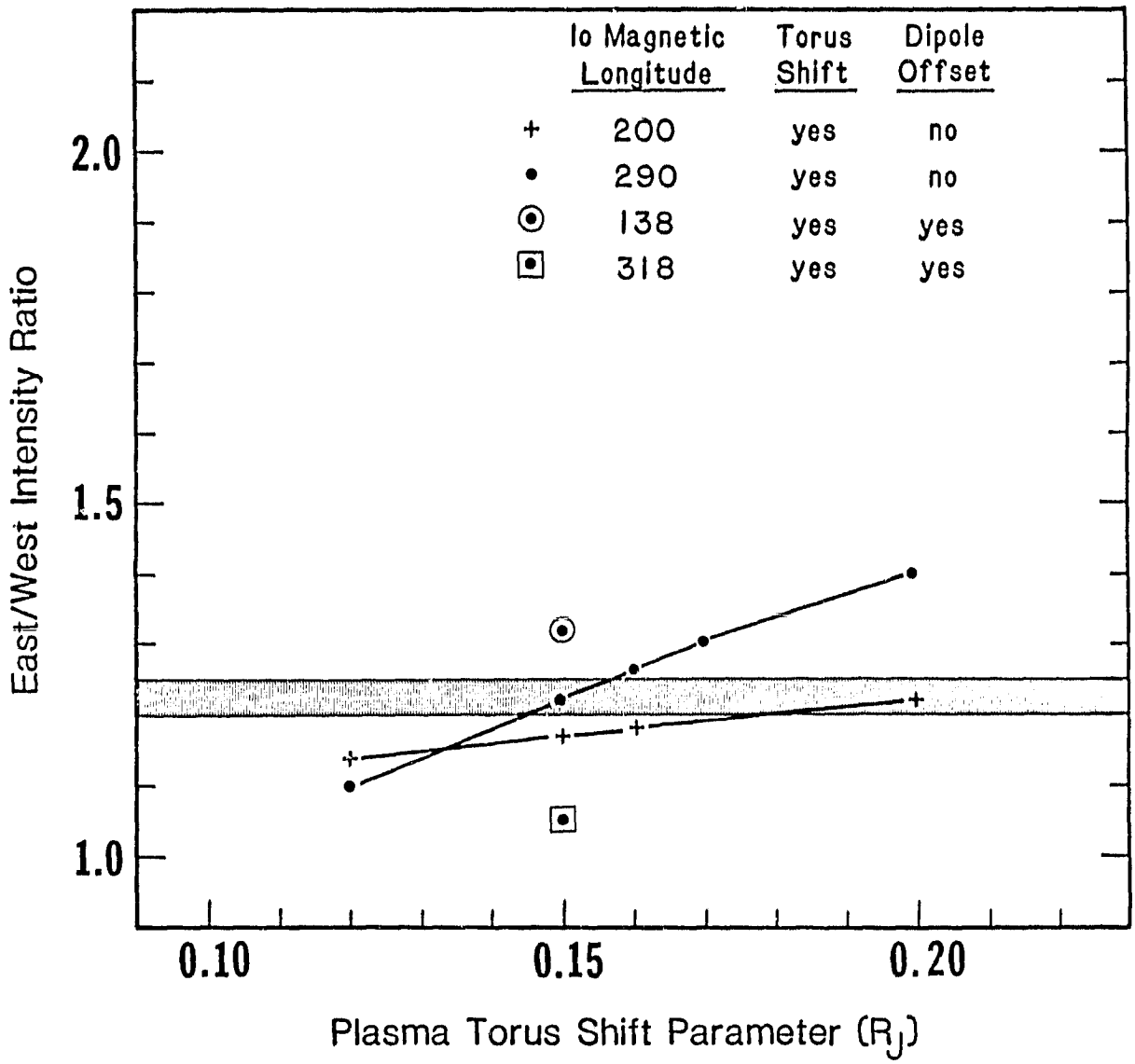

Figure 6. East-West Intensity Asymmetry of the Io Sodium Cloud.

The east-to-west intensity ratio measured by Bergstralh et al. (1975, 1977) is shown by the shaded area. Model calculations for different values of the plasma torus shift parameter are shown for various assumed physical conditions defined in the legend.

Figure 7

ELECTRON IMPACT IONIZATION LIFETIMES OF SODIUM AT IO'S POSITION

for an
East-West Electric Field and Offset Magnetic Dipole
(hours)

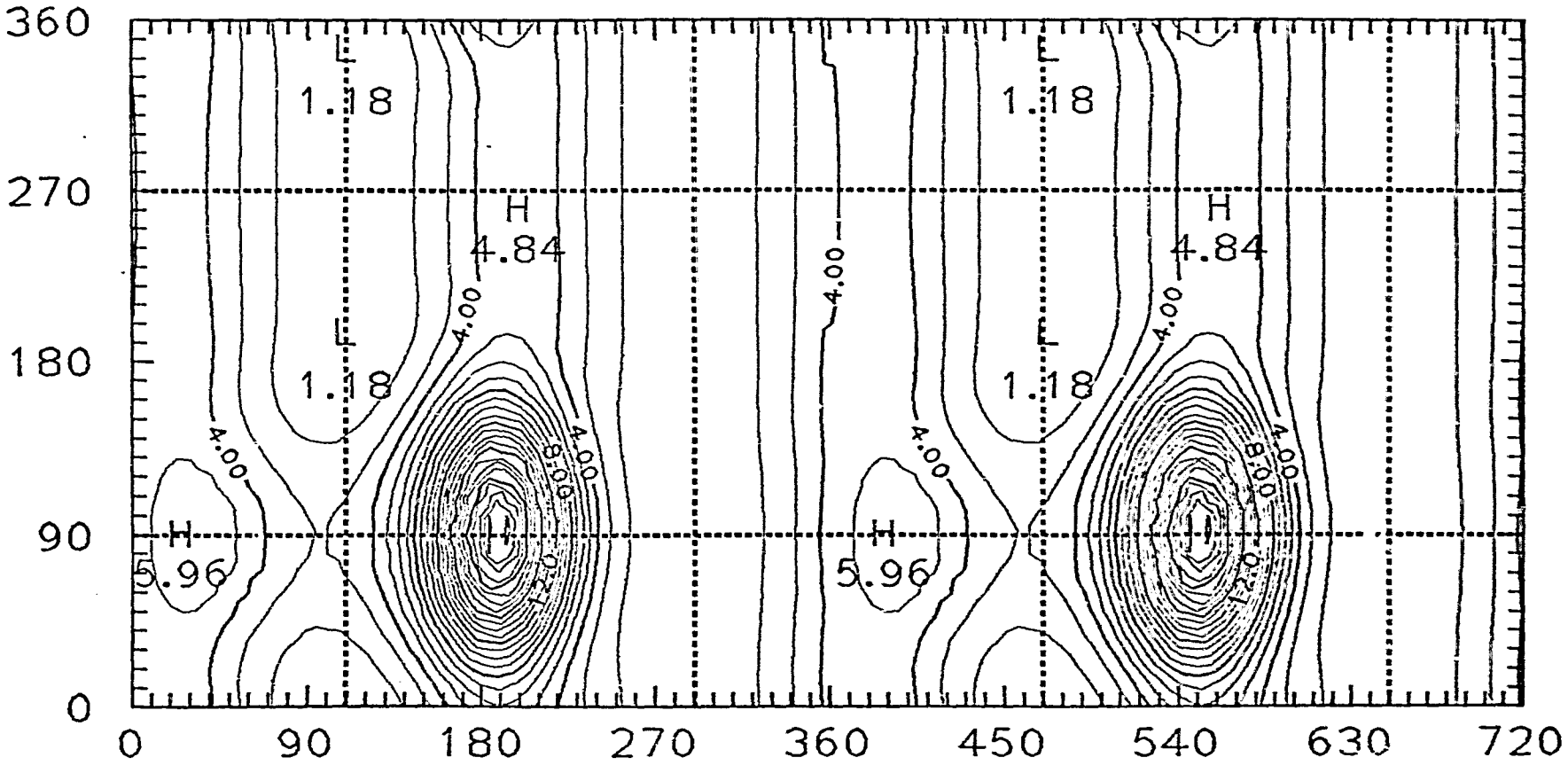

2.4 The Io Sodium Cloud: Region B

Model calculations for the spatial morphology of the Region B sodium cloud have been performed where effects of both the oscillating plasma torus sink and the acceleration of cloud atoms by solar radiation pressure in the D-lines have been included. Model calculations illustrating these effects for Io at both eastern and western elongation are shown projected onto the sky plane in Figure 8. These calculations assume radial and isotropic ejection of sodium from Io. Comparisons of model-calculated and observed (Murcray, 1978) D_2 images of the sodium cloud suggest a satellite source rate of 1-2 x 10^{26} atoms sec^{-1} for Region B. In Figure 8, the more elongated sodium cloud at western elongation results directly from the combined effects of orbit perturbations by solar radiation pressure and the spatially non-uniform lifetime of sodium in the plasma torus. This preferential elongation was anticipated by Smyth (1983) and has been observed for the sodium cloud (Goldberg et al., 1980; Goldberg, 1983). The model results in Figure 8 are displayed as they would appear above the satellite plane in Figure 9.

The preferential elongation of the sodium cloud in the west may be enhanced, however, by suitably modifying the ejection conditions of sodium from Io. This is illustrated in Figure 10, where sodium is ejected radially and uniformly only from the band region (defined in the Figure caption). This band ejection region is geometrically very similar to that deduced by Pilcher et al. (1984) as the source of high-velocity sodium (~20 km sec^{-1}) which can explain the space-time variations of the sodium directional features (Region C). The initial directions and speeds of sodium escaping Io that form the directional features were noted (Pilcher et al. 1984) to be understood in terms of a magnetospheric-wind-driven escape mechanism as discussed in the following section. Future modeling of data describing this east-west orbital asymmetry in the sodium cloud will allow a more refined description of the ejection conditions to be deduced. This information will then allow us to understand better the gas escape mechanism at Io as well as the properties of the local satellite atmosphere.

2.5 The Io Sodium Cloud: Region C

The directional features of the sodium cloud, discovered by Pilcher (see Hartline, 1980), extend from Region B into Region C. In the past year, the changing north-south directions of these features have been successfully

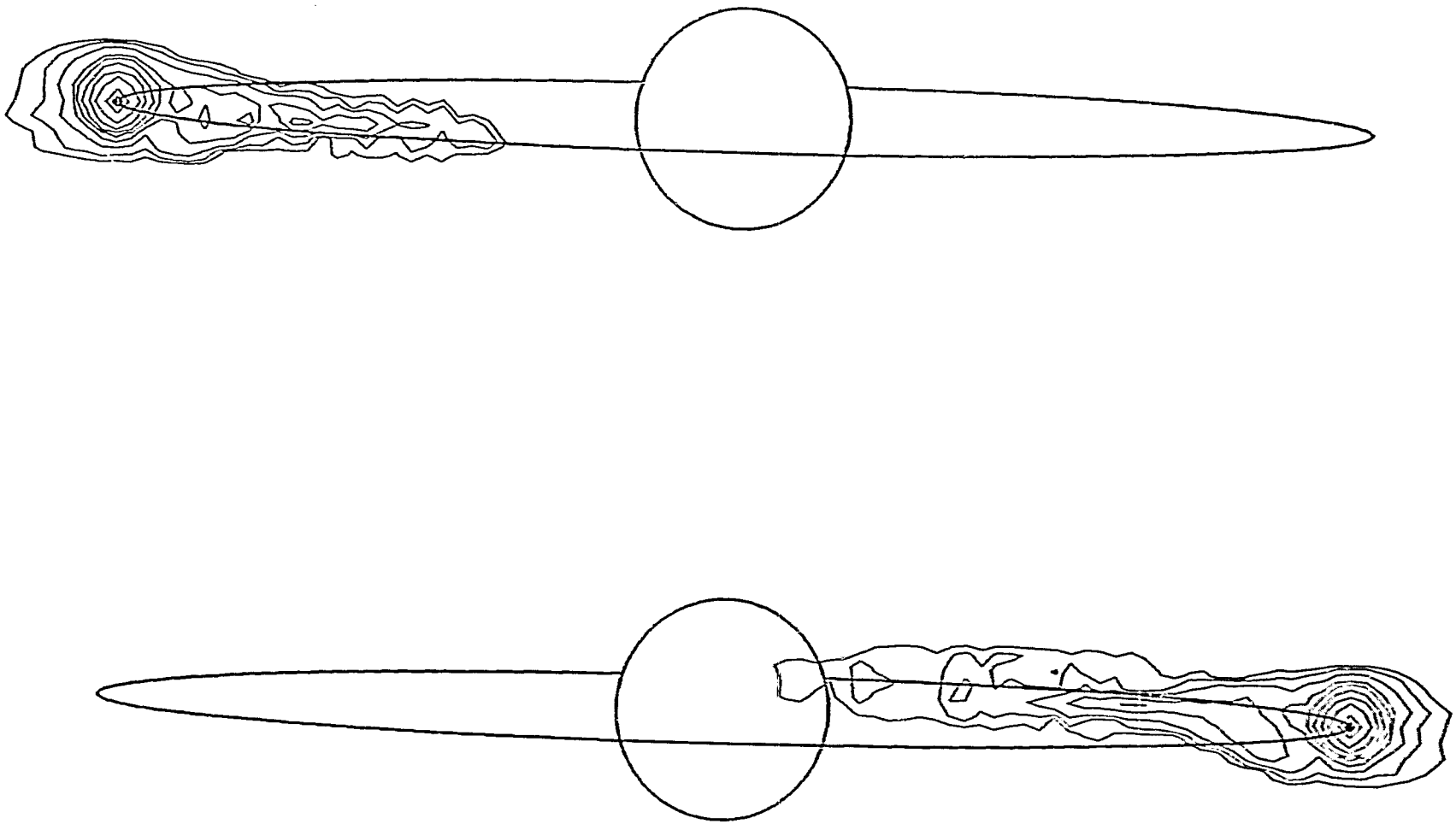

Figure 8. Model Calculation for the Io Sodium Cloud.

The calculation using the new AER model illustrates the D_2 emission line brightness on the sky plane produced when the oscillating plasma torus sink and solar radiation pressure are both included. The two calculations, for Io at orbital elongation and at a System III magnetic longitude of 200°, assume radial and isotropic ejection of sodium at 2.6 km sec^{-1} with a total source rate of 1.8×10^{26} atoms sec^{-1}. Contour values are, from outside to inside, 0.25, 0.5, 1, 2, 3, 5, 10, 20 and 50 kilo Rayleighs.

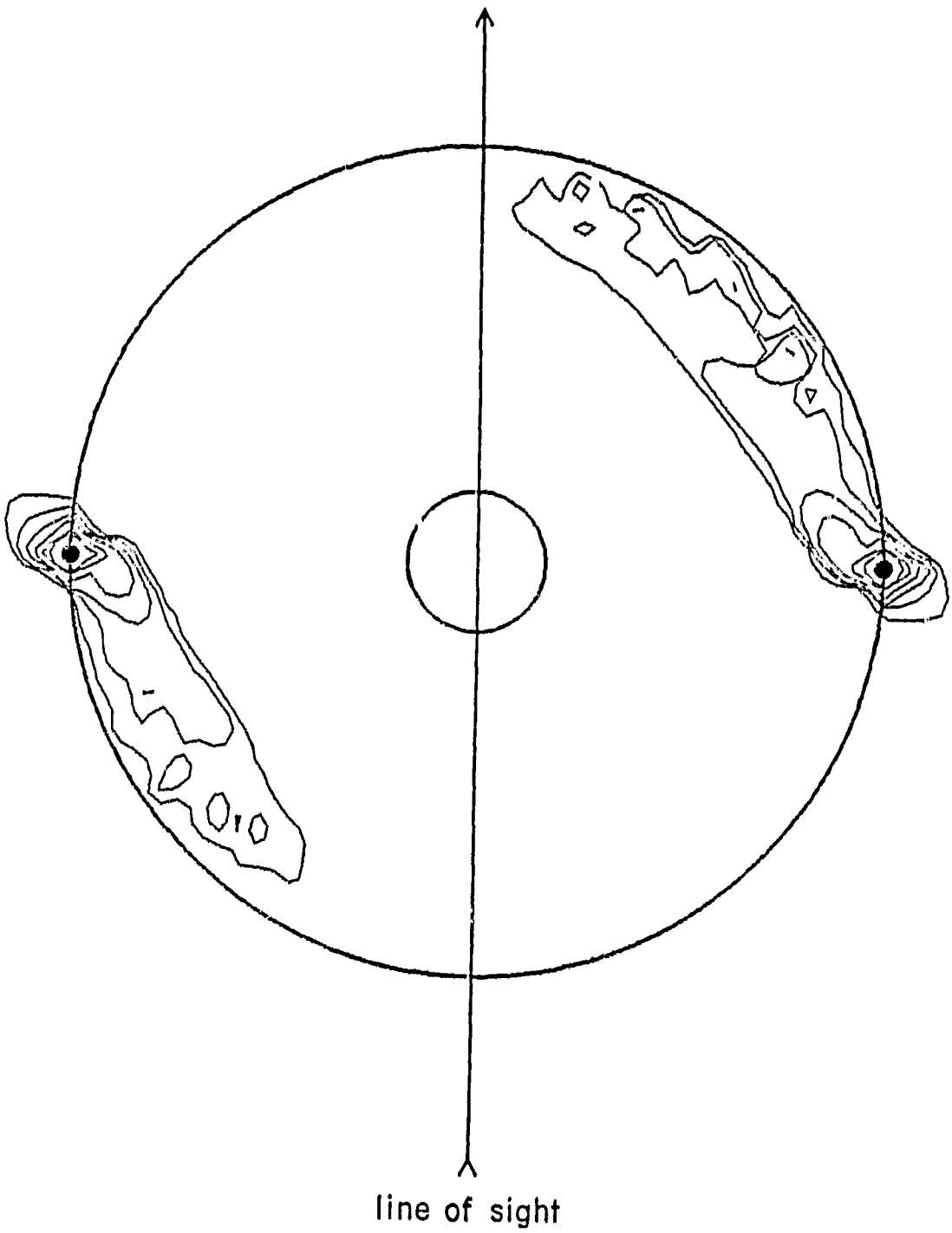

Figure 9 Model Calculation for the Io Sodium Cloud.

The calculations are the same two described in Fig. 8, but here show the D_2 emission intensity projected normal to the satellite plane. Contour values are, from the outside to inside, 0.1, 0.25, 0.5, 1,2,3 and 5 kiloRayleighs.

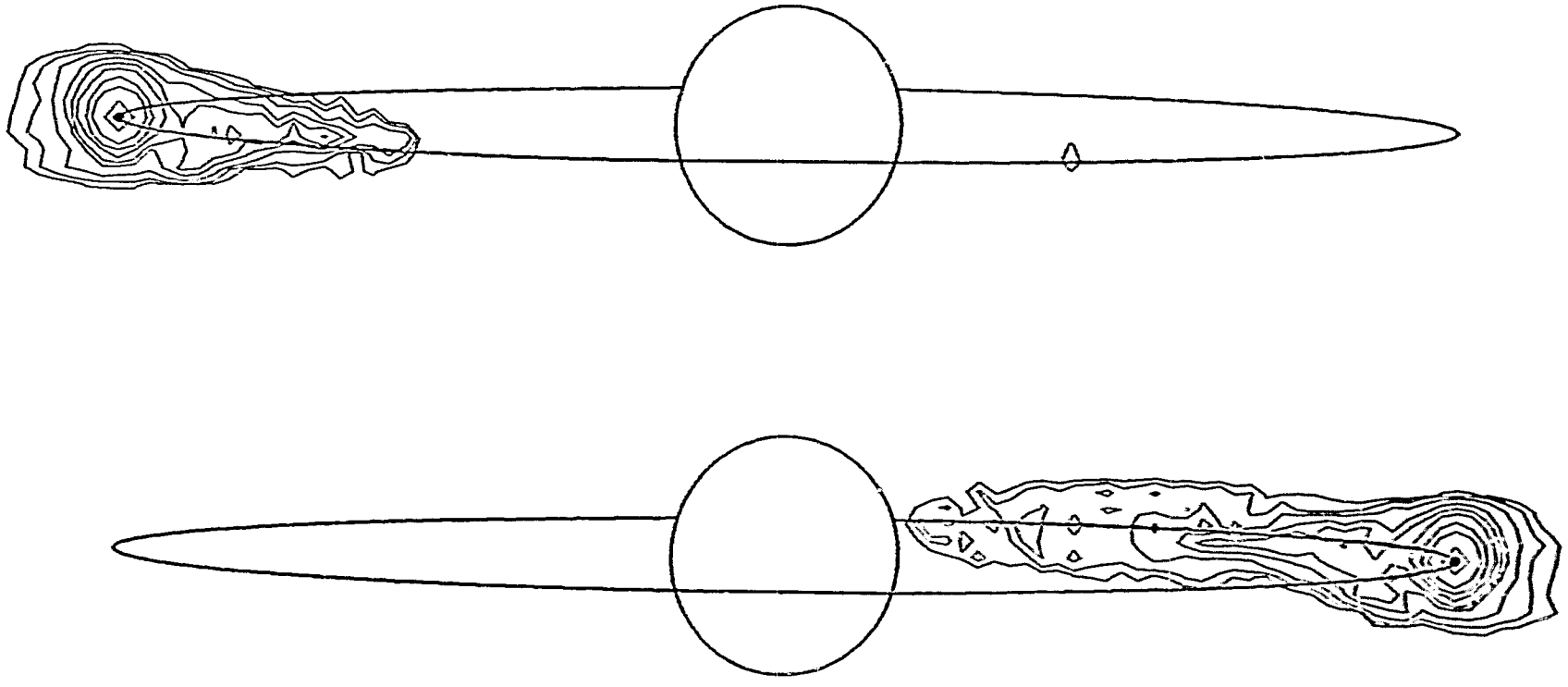

Figure 10. Model Calculation for the Io Sodium Cloud.

The calculation using the new AER model illustrates the D_2 emission line brightness on the sky plane produced when the oscillating plasma torus sink and solar radiation pressure are both included. The two calculations, for Io at orbital elongation and at a System III magnetic longitude of 200°, assume uniform and radial atom ejection at 2.6 km sec^{-1} from a symmetric band centered on the great circle normal to Io's orbital motion and having an angular width of ±40° and a total source rate of about 1.4×10^{26} atoms sec^{-1}. Contour values are, from outside to inside, 0.2, 0.5, 1, 2, 5, 10, 20, 50, and 100 kiloRayleighs.

understood through our model-data comparisons which have involved an active collaborative effort with Pilcher. The extremely interesting results of this collaborative effort are presented in the paper of Pilcher et al. (1984). This paper is accompanied by a companion paper entitled "Ejection of Atoms and Molecules from Io by Plasma-Ion Impact" submitted by Sieveka and Johnson (1984).

In short, the directional features can result from a source of high velocity (~20 km sec^{-1}) sodium combined with the oscillating neutral sodium sink provided by the plasma torus. The phase relationship between the features' directions and Io's magnetic longitude can be understood if escaping sodium is initially directed at near right angles to Io's orbital motion. The initial directions and speeds of sodium atoms escaping Io to form the directional features can be understood in terms of a magnetospheric-wind-driven escape mechanism. The companion paper of Sieveka and Johnson (1984) addresses the subject of ejection of sodium atoms from Io and provides support for the magnetospheric-wind-driven escape mechanism. The estimated satellite source for the directional features is ~1 x 10^{26} atoms sec^{-1} and is comparable to or slightly smaller than the Region B source deduced above. The similarity of these two source rates for very different velocity ranges of the ejected atoms provides additional diagnostic characteristics (as noted by Sieveka and Johnson, 1984) that characterize the magnetospheric-wind-driven escape mechanism.

2.6 The Io Potassium Cloud

The Io potassium cloud has been observed to radiate in the 7665 Å and 7699 Å lines by Trafton (1975) and in the 7699 Å line by Trauger, Roesler and Münch (1976; Münch, Trauger and Roesler, 1976). The radiation is thought to arise from solar resonance scattering. Additional observations of Trafton (1977, 1981) have shown that the Io potassium cloud exhibits spatial and temporal variations similar to those observed for the sodium cloud. These observations indicate that the potassium cloud undergoes periodic fluctuations in response to solar radiation pressure (producing the east-west asymmetries) and in response to the ionizing influence of Jupiter's plasma torus (producing the north-south asymmetries). In addition, temporary directional features of potassium from Io have also been observed. Modeling improvements for the sodium cloud model discussed in the preceding subsection may therefore be incorporated directly in the Io potassium cloud model.

An Io potassium cloud model has been developed this year. It includes the electron impact ionization lifetime of potassium in the oscillating plasma torus (see Figure 11), the solar spectrum for each potassium line (see Figures 12 and 13), and the acceleration experienced by potassium atoms as they undergo solar resolnance scattering. The electron impact ionization of potassium in Figure 11 is comparable to the sodium lifetime in Figure 1 in both magnitude and spatial character. Both of the potassium lines appear in solar absorption features, and the line at 7665 Å is almost completely obscured to a ground-based observer because of an optically thick oxygen absorption feature present in the earth's atmosphere. To properly model the intensity morphology of the cloud or the line profile shape in the 7665 Å emission, the exact shape of the solar absorption feature above the earth's atmosphere must be known as well as the relative motion between the cloud atoms and the Earth. The computation of the unobstructed solar abosrption feature and the earth's atmospheric transmission function was provided in the first program year by Kurucz (1982), with whom a collaborative effort for this purpose was established. The results of his computations are shown in Figures 12 and Figure 13 and have been adopted in the model calculation to determine both the excitation rates and the atom accelerations produced by solar resonance scattering. Because of the differences in the shapes of the potassium and sodium absorption features, the maximum magnitude of the acceleration produced by solar radiation pressure is in fact comparable. In modeling, therefore, the Io potassium cloud should exhibit east-west asymmetries of similar magnitude to those calculated earlier for the sodium cloud.

Model calculations for the brightness of the Io potassium cloud in the 7665 Å emission line at both eastern and western elongations are shown in Figure 14. These calcluations include the oscillating plasma torus and assume isotropic ejection of potassium at 2.6 km sec^{-1} from Io's exobase. Adopting a brightness of about 100±50 Rayleighs near Io as reported by Trafton (1981), a potassium flux of 1.2×10^7 atoms $cm^{-2}sec^{-1}$ (relative to Io's surface) or a total source rate of about 5×10^{24} atoms sec^{-1} is required by the model. The results in Figure 14 have used this source rate and are for Io at a system III magnetic longitude of 200°. Solar radiation pressure is responsible for the shorter cloud in the east and the longer cloud in the west. This value of the potassium source rate is about a factor of 20-40 smaller than the sodium source rate deduced for Region B and is similar to that expected based upon the relative cosmic abundance of the two elements.

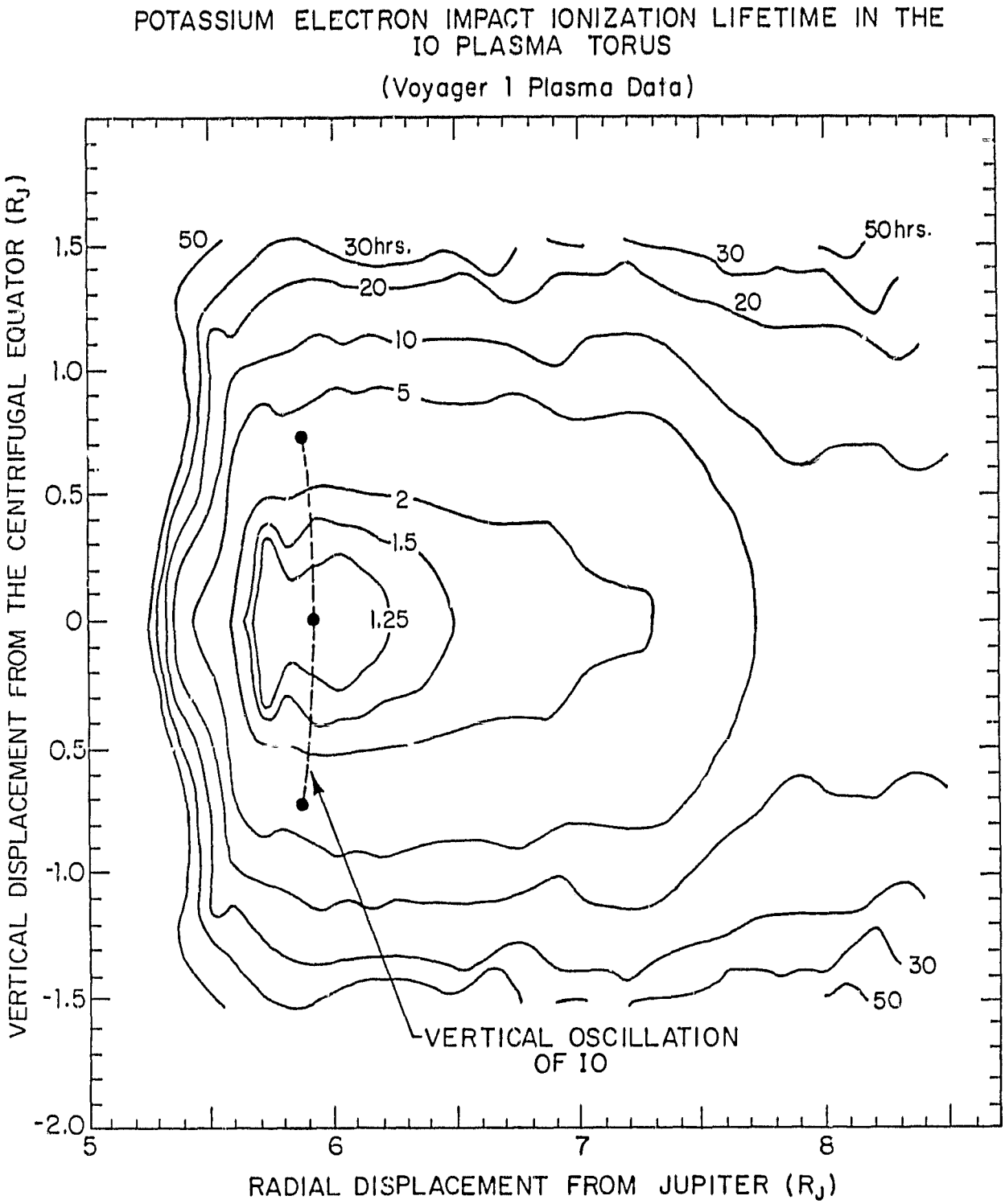

Figure 11. Potassium Electron Impact Ionization in the Io Plasma Torus.

The lifetime calculation is based upon the cross-section measured by McFarland (1965), McFarland and Kinney (1965), and Zapesochnyi and Aleksakhin (1968), Voyager 1 in situ measurements of the plasma density (Bridge, Sullivan and Bagenal, 1980; Bagenal and Sullivan, 1981), and Voyager 1 UVS (Shemansky, 1980) and in situ measurements (Scudder, Sittler and Bridge, 1981) for the electron temperature. The two-dimensional common temperature model of Bagenal and Sullivan (1981) was selected to describe the electron density.

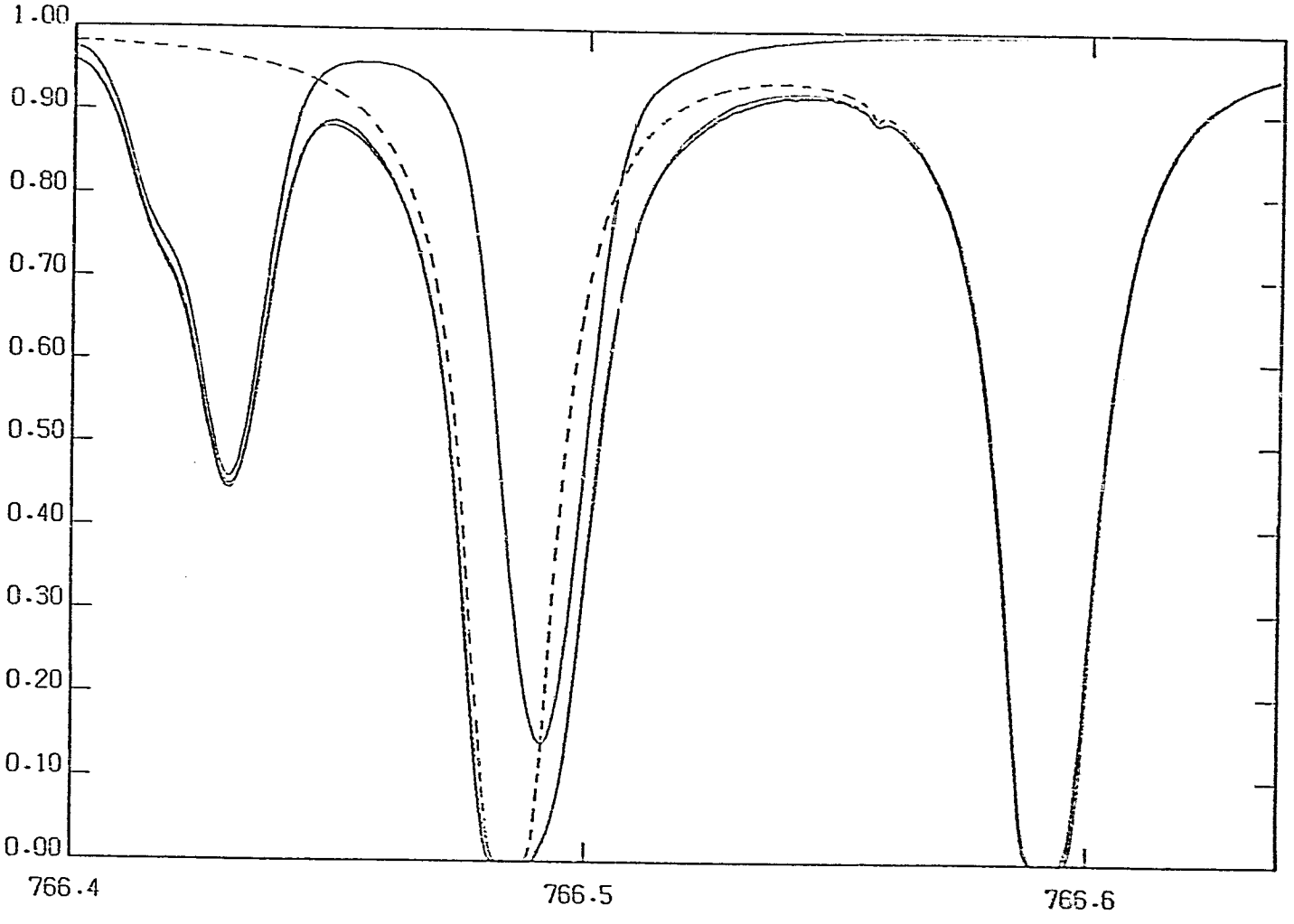

Figure 12. Solar Spectrum and Earth's Atmospheric Transmission Function for the 7665 Å Potassium Line.

The solar spectrum above the earth's atmosphere, indicated by the light-weight line (not the one plotted very near the heavy-weight line), and the earth s atmospheric transmission function for the location of the Kitt Peak Observatory, indicated by the dashed line, were both calculated by Kurucz (1982). The solar spectrum observed at the location of the Kitt Peak Observatory is indicated by the heavy-weight line and the predicted shape of this spectrum (Kurucz, 1982) by the light-weight line that is plotted very near the heavy-weight line.

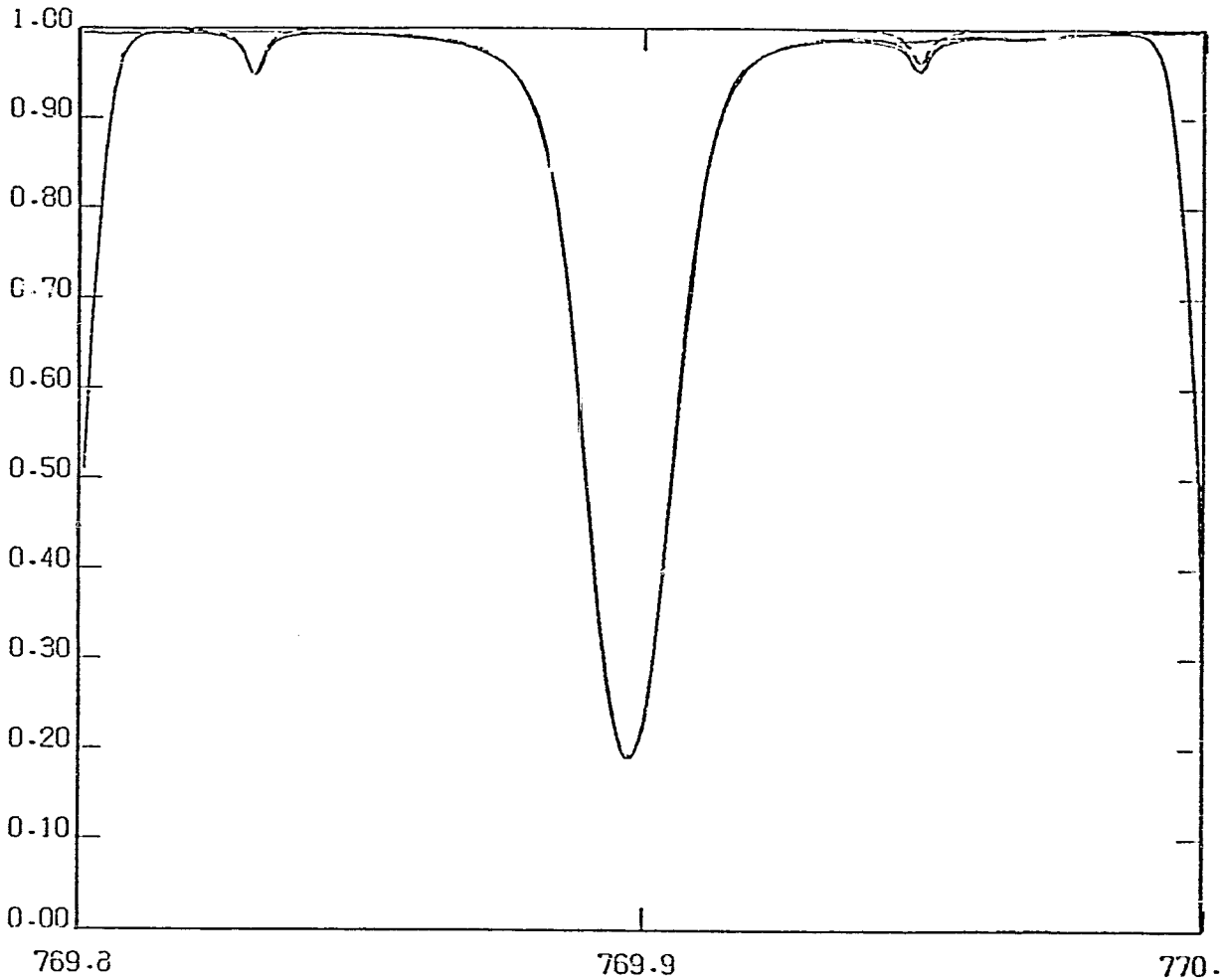

Figure 13. Solar Spectrum and Earth's Atmospheric Transmission Function for the 7699 Å Potassium Line.

The solar spectrum above the earth's atmosphere, indicated by the light-weight line, and the earth's atmospheric transmission function for the location of the Kitt Peak Observatory, indicated by the dashed line, were both calculated by Kurucz (1982). The solar spectrum observed at the location of the Kitt Peak Observatory is indicated by the heavy-weight line and the predicted shape of this spectrum (Kurucz, 1982) in the plot is indistinguishable. The downward trend of the spectrum on the left and right boundaries of the plot is instrumental in origin.

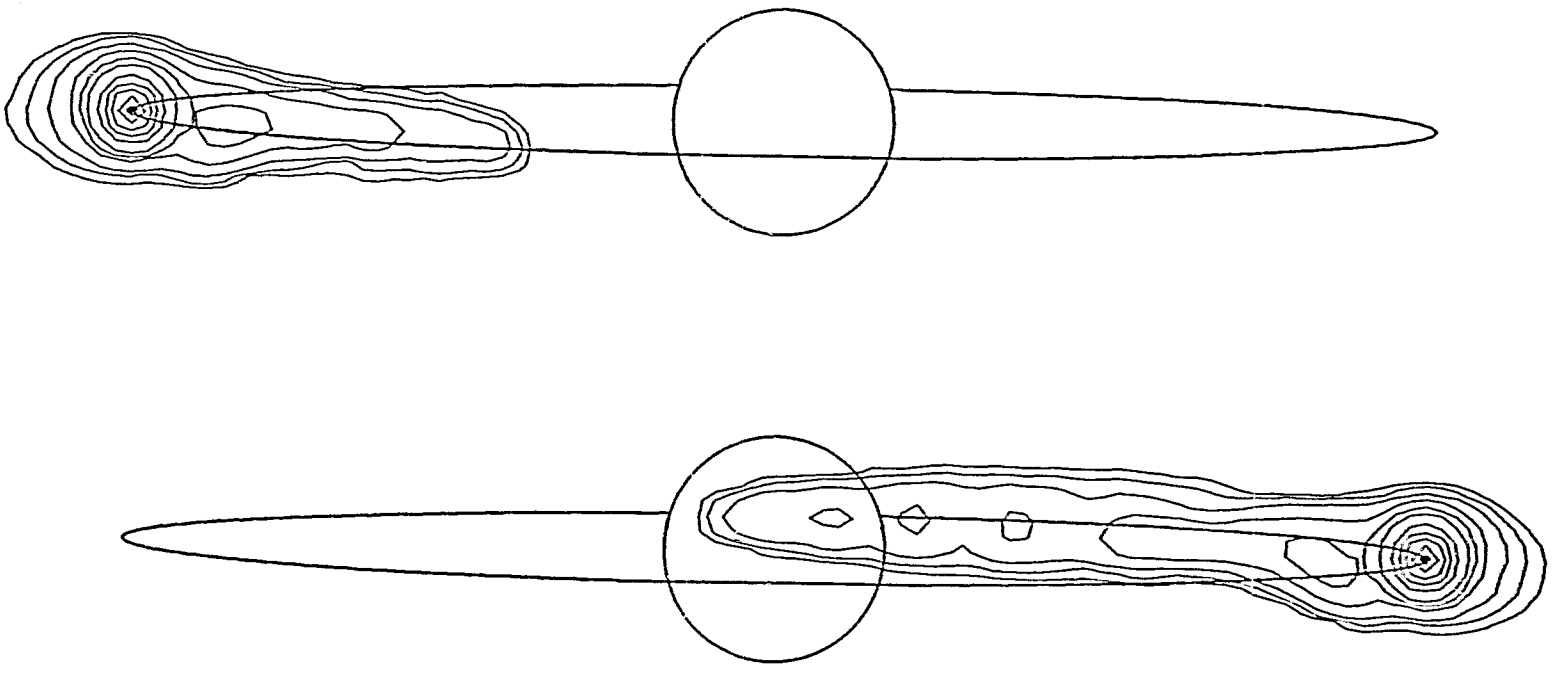

Figure 14. Model Calculation for the Io Potassium Cloud

The calculation using the new AER model illustrates the 7665 Å emission line brightness on the sky plane produced when the oscillating plasma torus sink and solar radiation pressure are both included. The two calculations, for Io at orbital elongation and at a System III magnetic longitude of 200°, assume isotropic and radial atom ejection at 2.6 km sec^{-1} and a total source rate of 3 x 10^{24} atoms sec^{-1}. Contour values are, from outside to inside, 5, 10, 20, 50, 100, 200, 500, 1000 and 1500 Rayleighs.

III. THE SATURN SYSTEM

3.1 Introduction

For the Saturn system, a condensed summary of our three year research program is given in Table 2. The four subtopics listed in Table 2 represent four plausible sources of hydrogen for the Saturn system. Efforts in the first year of this research program were directed primarily to the planetary ring atmosphere, where new data had become available from the Voyager 1 and Voyager 2 encounters. In the second year, the planet was recognized as being a possible source of H for the larger Saturn system (Shemansky and Smith, 1982), and the scope of the problem has been appropriately broadened and refocused as indicated by the addition of the first topic in Table 2. An extended hydrogen atmosphere for Saturn must now be considered as a plausible source of H atoms previously interpreted as a planetary ring atmosphere and might even be an important source for some of the hydrogen previously associated with a Titan source.

To further explore and understand this subject, our past collaborative effort with D. E. Shemansky (regarding the Titan torus data obtained by the UVS instrument of the Voyager spacecraft) was expanded in scope. The first step in the expanded collaboration with Shemansky has been to begin to update the Titan model of Smyth (1981) to include the lifetime processes (electron impact ionization, charge exchange, and photoionization) for hydrogen operative in Saturn's magnetosphere. Model calculations of the Lyman-α intensity in the magnetosphere produced by H atoms lost by Titan may then be properly calculated and compared to the UVS measurements of the Voyager spacecraft. Such analysis will allow us to determine if gases from the E-ring icy satellites (for which spatial gas envelopes are illustrated for Tethys and Dione in Figure 15) or from the planet are relevant in understanding the Voyager UVS data. Specific efforts to accomplish these objectives in the third year are discussed below.

3.2 The Role of Titan and Non-Titan Sources

Efforts in the past year toward understanding the role of Titan (and hence non-Titan sources) in the production of Saturn's hydrogen torus have centered about (1) gathering information necessary to specify the plasma conditions operative at Saturn, (2) calculating the hydrogen lifetime in the planetary magnetosphere, and (3) improving the previous Titan hydrogen model

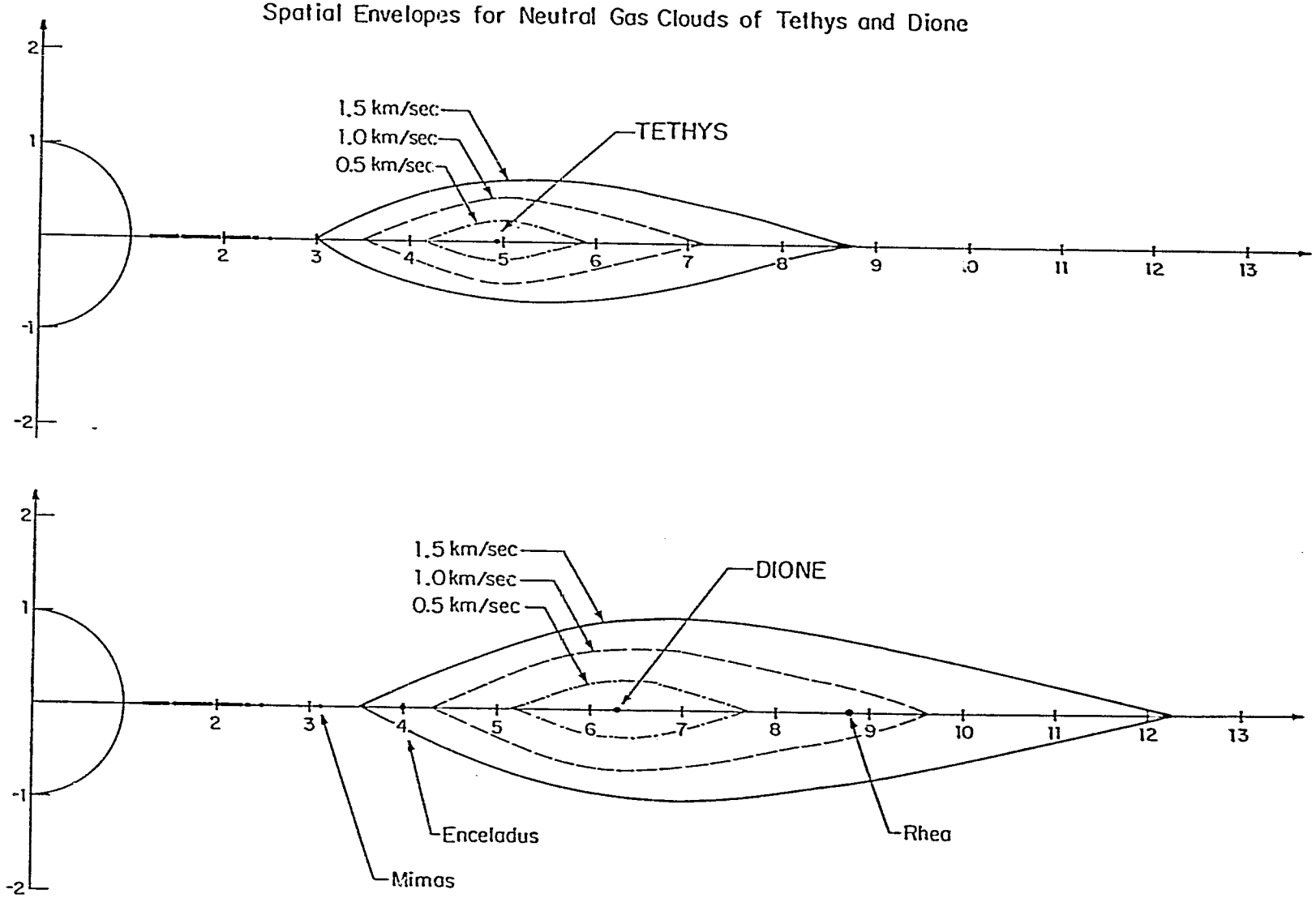

Figure 15. Spatial Envelopes for Neutral Gas Clouds of Tethys and Dione.
The spatial envelope that contains gas atoms emitted from the satellite with velocities of 0.5, 1.0 and 1.5 km/sec is shown in relation to Saturn, the main planetary rings and other E-ring icy satellites.

of Smyth (1981) by incorporating this spatially varying sink. Progress in these areas was presented as an exhibit at the American Astronomical Society 16th annual meeting of the Division for Planetary Science (Shemansky, Smith, Smyth and Combi, 1984). Plasma information for the planetary magnetosphere has been obtained after considerable processing of Voyager PLS data from Edward C. Sittler (Goddard Space Flight Center), who has recently become part of this larger collaborative effort. The electron and ion densities and temperatures along the spacecraft trajectory have been used to generate a two-dimensional (longitudinally symmetric) description of the planetary magnetosphere. Further Voyager PLS data have been used to describe solar wind and magnetospheric tail plasma conditions. In the magnetosphere, both a cold and a hot component of electrons are included and both light (H^+) and heavy ions (O^+ and N^+) are considered.

Lifetime processes for atomic hydrogen in the Saturnian system are summarized in Table 3. Using the Voyager 1 outbound plasma data, the lifetime of hydrogen in Saturn's equatorial plane is shown in Figure 16 and compared with the solar wind charge exchange and photoionization lifetime of H atoms. The lifetime value assumed in the earlier Titan torus model calculations of Smyth (1981) is also shown. The lifetime decreases fairly rapidly for departures normal to the equatorial plane. With the exception of atomic hydrogen located inside a radial distance of 10 Saturn radii (R_S), the lifetime based upon the Voyager 1 data is larger than that assumed earlier by Smyth (1981). This implies that the nearly longitudinally symmetric distribution of H atoms about Saturn (see Figure 17) calculated earlier by Smyth (1981) will remain and, to first order, will be only altered in its radial profile by the spatially varying lifetime for H atoms. This alteration is, however, most important since it will allow us to divide the Voyager UVS Lyman-α brightness data (see Figure 18) into a Titan and non-Titan H source.

The full two dimensional lifetime of H atoms in the Saturn environment has been incorporated in the earlier model of Smyth (1981). Preliminary testing of the model was in progress at the close of this project year. This work is to be continued under new NASA support and definitive results are anticipated in the near future.

Table 3

LOSS PROCESSES FOR ATOMIC HYDROGEN IN THE SATURNIAN SYSTEM

1. $H + \left\{ \begin{array}{ll} e & \text{(cold)} \\ e & \text{(hot)} \end{array} \right\} \longrightarrow H^+ + 2e$

2. $H + \left\{ \begin{array}{l} H^+ \\ O^+ \\ N^+ \end{array} \right\} \longrightarrow H^+ + \left\{ \begin{array}{l} H \\ O \\ N \end{array} \right\}$

3. $H + h\nu \longrightarrow H^+ + e$

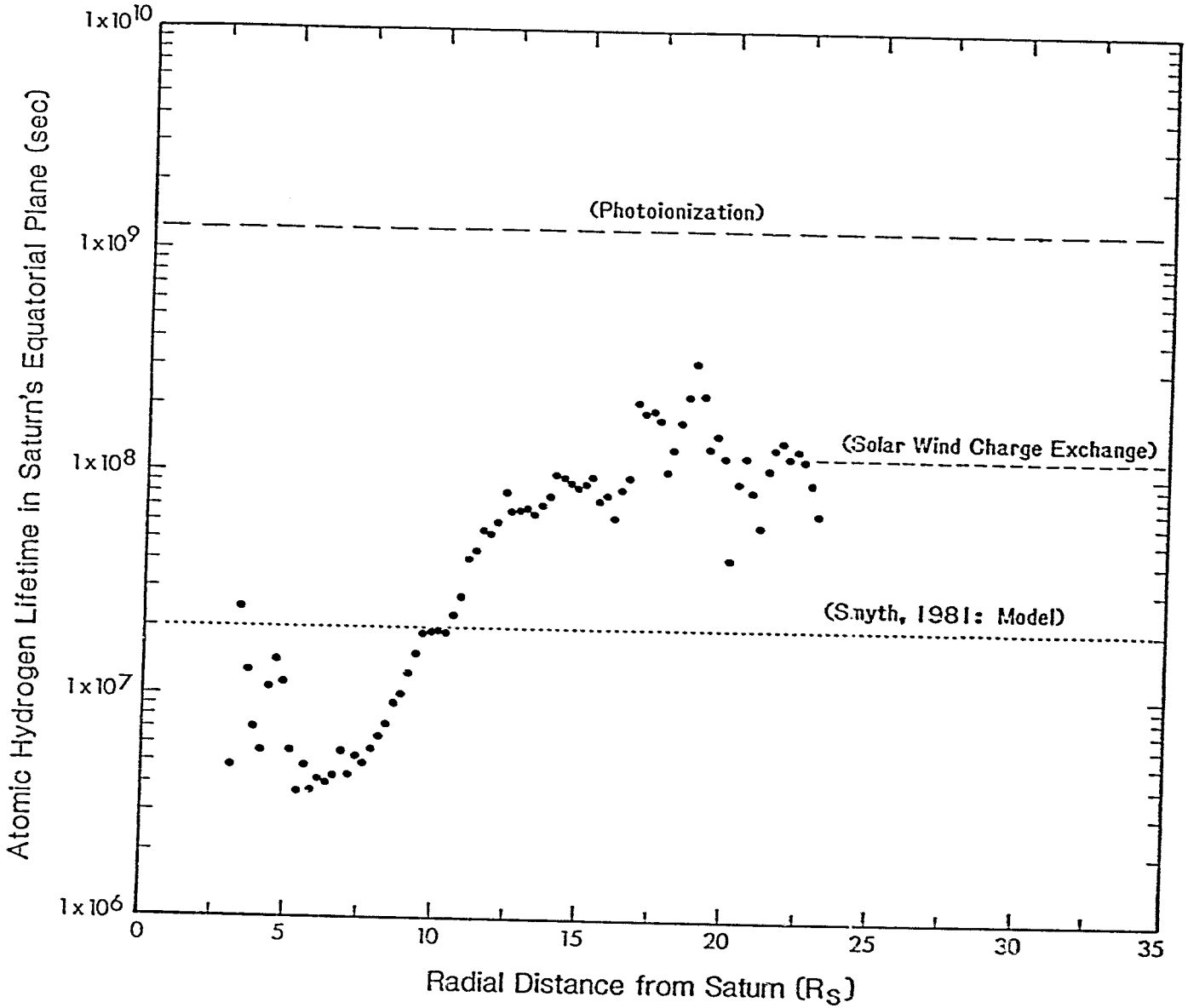

Figure 16. Lifetime of Atomic Hydrogen in Saturn's Magnetosphere. The lifetime is appropriate for the reactions of Table 3 and the plasma information based upon an analysis of the Voyager PLS data by Sittler (1984).

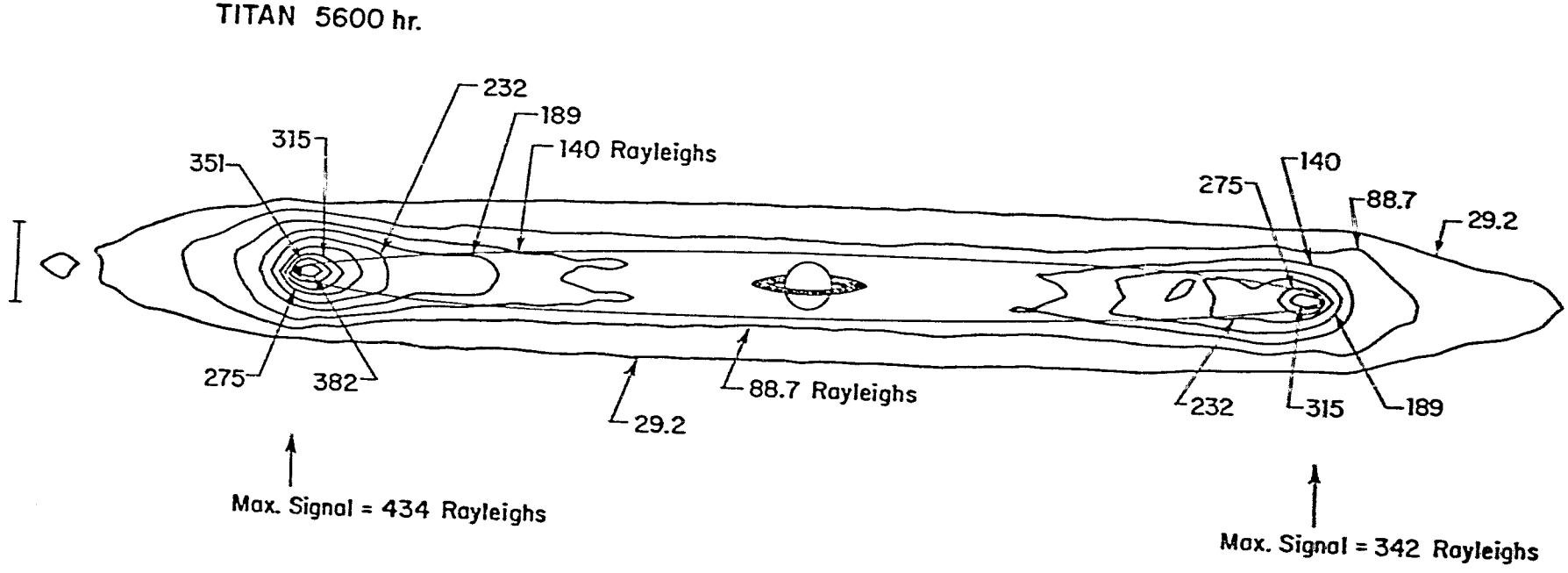

Figure 17. Model Calculation of Lyman-α Emission from the Titan Hydrogen Torus. Intensity contours, calculated assuming resonance scattering of sunlight, are shown for the satellite plane tilted by 3.25°. An isotropic emission of H atoms with an initial speed of 2.0 km s^{-1}, a satellite flux of 3×10^9 cm^{-2} s^{-1} and the indicated lifetime were assumed.

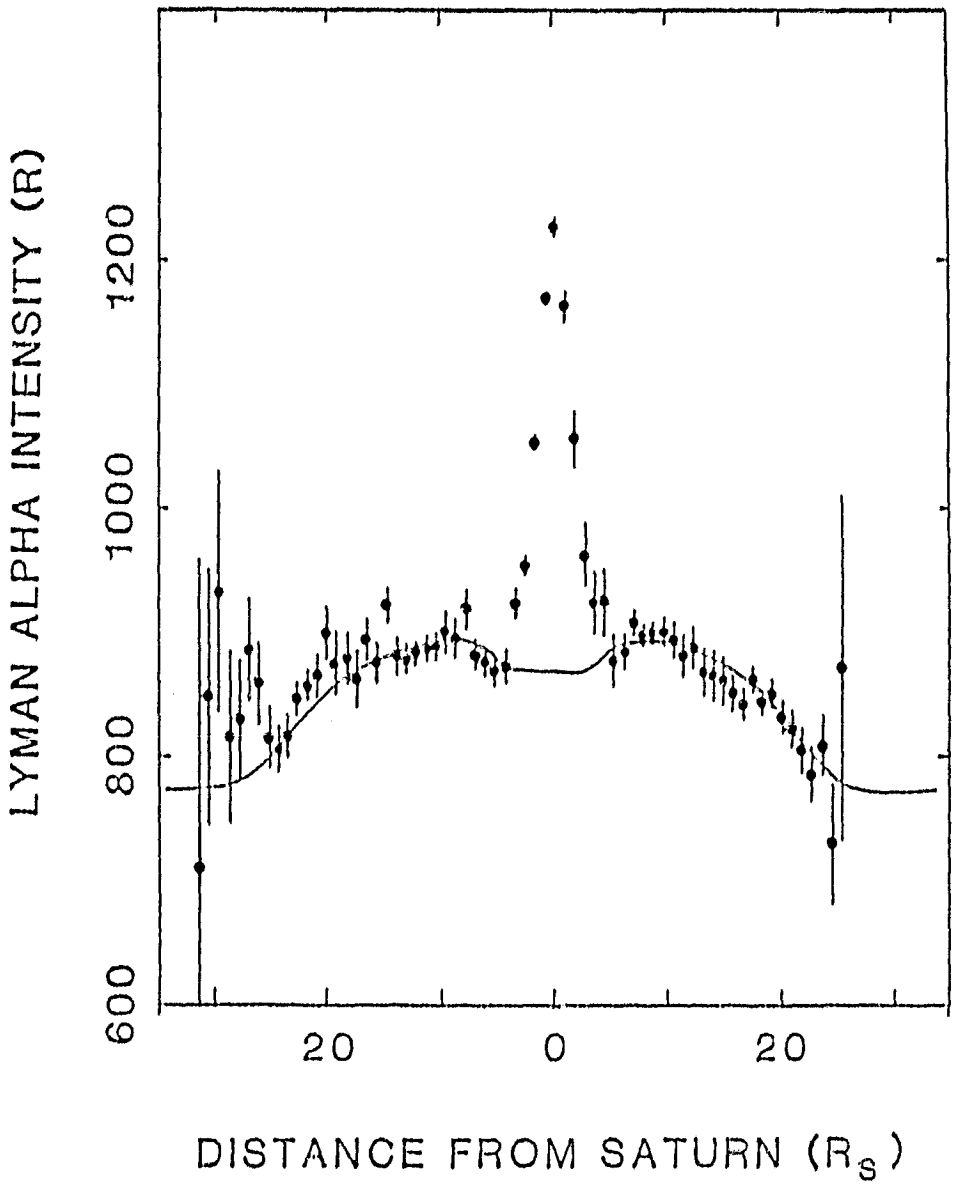

Figure 18. Model vs. UVS Lyman-α Scan of the Hydrogen Torus.

The Voyager 1 UVS Lyman-α radial scan and a solid line for the simple constant density torus model of Broadfoot et al. (1981) is shown. The central peak in the data points is due to the convolution of Saturn's Lyman-α disk by the UVS slit.

IV. COMETARY ATMOSPHERES

4.1 Introduction

Cometary research at AER represents a broadening and natural extension of our previous modeling of extended satellite atmospheres, that was initially undertaken for NASA in 1979 and 1980. Because of the expertise developed at AER in modeling extended satellite atmospheres, which are in a collisionless regime but remain in a complex gravitation field, we have addressed that area of cometary atmospheres where similar conditions are present. The three dimensional particle trajectory model developed at AER earlier is now being applied to the extended neutral gas clouds observed in comets (e.g. H, C and O). In particular, we have constructed a model for the observed spatial distribution of cometary hydrogen. The AER three dimensional particle trajectory model is ideally suited to modeling cometary H atoms which travel under the influence of the solar gravitation field and a variable solar radiation pressure field owing to resonance scattering of solar Lyman α photons.

The general state of extended cometary gas cloud models has been one in which sets of simplifying assumptions are made to tailor the models to one particular aspect of observational data. The two major and somewhat complementary modeling efforts to date have been put forth by Keller and his co-workers (Keller and Thomas, 1975, Keller and Meier, 1976) and Festou et al. (1979). Keller and co-workers have developed models for the extended H cloud ($>10^6$ km) that approximate the source region as a point. These models, however, use Maxwell-Boltzmann velocity distributions and various approximation schemes to calculate atom trajectories under the influence of the solar gravitational field and solar radiation pressure. Festou et al. (1979) have used the vectorial model (Festou 1981 a,b) to describe more realistically the source region of H in their analysis of the inner coma ($\sim 10^4$ km) Lyman α profiles from Comet Kobayashi-Berger-Milon (1975 IX). Their model assumed a steady state production rate and neglected (appropriately for these particular observations) the effects of the solar gravity field and solar radiation pressure.

4.2 The Particle Trajectory Model

Particle trajectory models are not limited to certain spatial regions, as in previous modeling efforts. They can be used to calculate correctly the three-dimensional atom trajectories in an arbitrarily large spatial domain

($> 10^6$ km) and at the same time to describe properly the spatially extended source region (10^4 - 10^5 km).

Particle trajectory models have already been successfully applied to the analysis of neutral radical distributions (10^4 to several times 10^5 km). Combi and Delsemme (1980) introduced a Monte Carlo particle trajectory model to treat correctly the isotropic ejection of daughter radicals upon photodissociation of the parent molecules. This model is based therefore on the same accurate spatial distribution and kinematics as the vectorial model of Festou (1981a) which was developed at the same time but independently. It differs, though, in that it does not involve the lengthy multiple-numerical integration, is easily generalizable and provides a two-dimensional description of the coma to include properly the effect of solar radiation pressure. Combi (1980) applied this model with solar radiation pressure to analyze sunward and antisunward profiles of CN in Comets Bennett (1970 II) and West (1976 VI).

The cometary hydrogen cloud model, developed at AER, calculates the atom trajectories in three dimensions by integrating Newton's equation with a fourth order Runge-Kutta routine and includes both the solar gravitational field and variable solar radiation pressure. The characteristics adopted for the source region (that is, the starting location and velocity of the H atom with respect to the nucleus) are those appropriate for the two step photodissociation of H_2O as described by the Monte Carlo particle trajectory models of Combi and Delsemme (1980). The trajectory calculation explicitly includes the orbital elements of the comet, and the absolute time of the observation. The placement of an atom on the sky plane is calculated taking into account the divergent lines of sight (parallax) appropriate for the relative comet-sun-earth geometry. The decay lifetimes of the parent molecules for H (H_2O and OH) are handled in the manner described by Combi and Delsemme (1980), but the decay of H, being much larger and having stronger time dependence through the changing heliocentric distance, is calculated explicitly in the trajectory time-step routine to properly include its spatially changing lifetime.

The variable radiation pressure acceleration on H atoms as well as the instantaneous emission rate of Lyman-α at the observation snap shot are calculated in the model from the solar disk averaged Lyman-α profile of Lemaire et al. (1978). The solar profile is shown in Figure 19. The Lyman-α absorption rate by a cometary H atom is a function of the heliocentric velocity

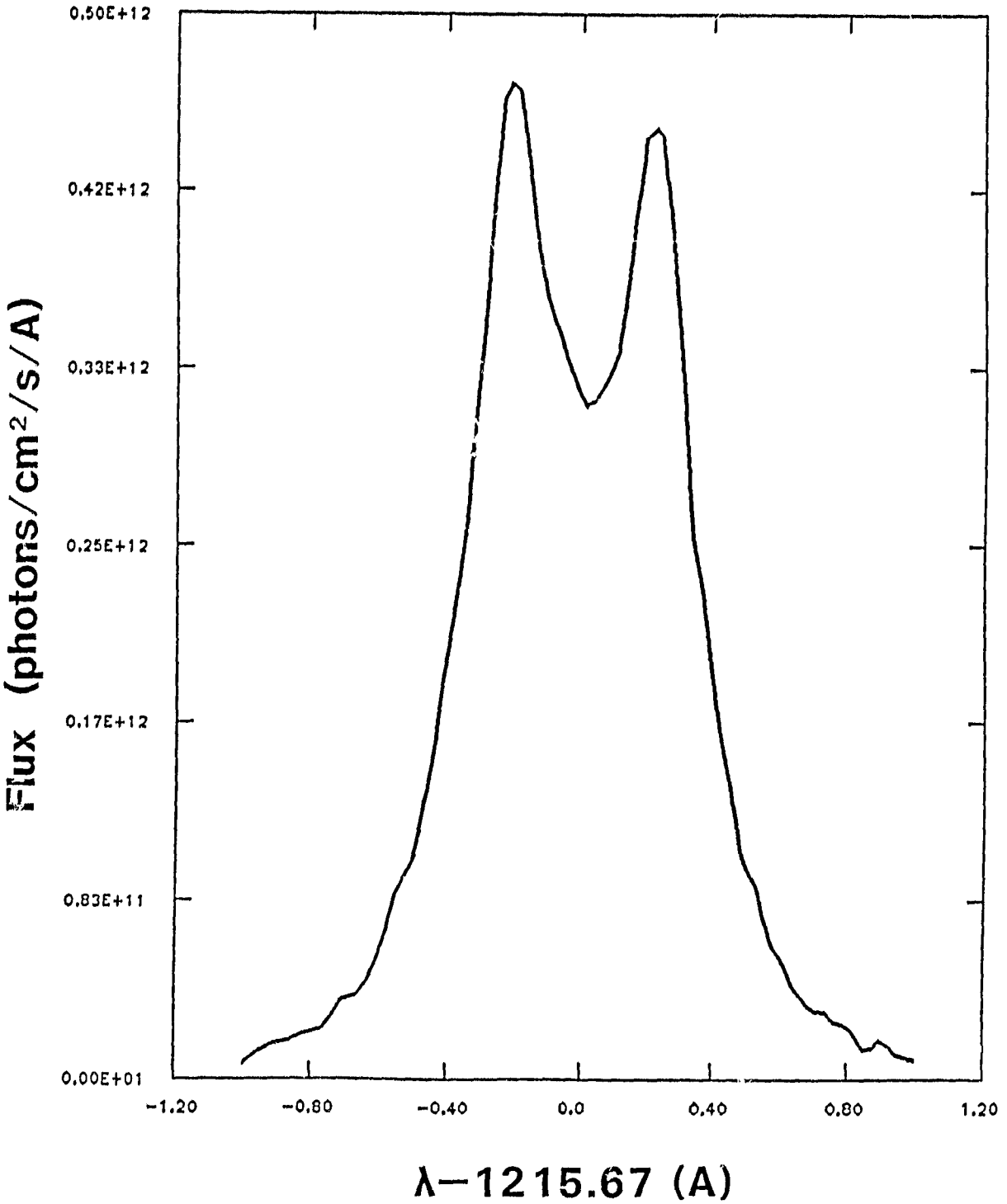

Figure 19. Full Solar Disk Lyman-α Line Profile.
The profile was determined by Lemaire et al. (1978).

(i.e., the position along the profile) as well as the inverse square of the heliocentric distance.

4.3 Model Applications

As a test of the new hydrogen model, we have begun re-analyzing the observed Lyman-α distribution of Comet Kohoutek (1973 XII). These data were first analyzed by Meier et al. (1976) with their model that was discussed in the previous section. They found they could fit the observed isophotes with an isotropic point source of three Maxwell-Boltzmann distributions having rms velocities of 4, 8 and 20 km s^{-1}. This velocity distribution can roughly be understood in terms of H production from water photodissociation by solar UV radiation (Keller and Meier, 1976; Festou et al., 1979). Table 4 shows the branching ratios and product velocities for H and OH corresponding to photodissociation of H_2O. The major component is in fact at 20 km s^{-1}. The 8 km s^{-1} component is now clearly understood to result from the photodissociation of OH (Jackson, 1980; Schleicher and A'Hearn, 1983; van Dishoeck and Dalgano, 1984). The 4 km s^{-1} component had been suggested by Meier et al. to result from thermalization of a fraction of the H which was actually produced within the collision zone. This low velocity component of H was required for smaller heliocentric distances where the gas production rates were higher and corresponding decay scale lengths were shorter. This has been demonstrated more conclusively by Kitamura et al. (1983).

Festou et al. (1979) used a velocity distribution as expected from photodissociation with narrow peaked components at 8 and 20 km s^{-1} which were naturally broadened by the spatially extended isotropic dispersion of the vectorial model. We have chosen this type of physically motivated picture as a starting point for our modeling analysis. Figure 20 shows a contour plot of the Lyman-α emissions from Comet Kohoutek (1973 XII) on January 8, 1974 from the original paper by Meier et al. (1976).

Instead of assuming a simple r^{-n} law for the production rate of H_2O, in our model we have adopted the vaporization curves of Delsemme (1976) as fitted to the visual light curves of Comet Kohoutek (see Figure 21). The parent H_2O molecules are assumed to flow isotropically from a point source with a velocity of 0.58 $r_H^{-0.5}$ in km s^{-1}, where r_H is in AU (Delsemme, 1982; Whipple,

Table 4

Photoabsorption of Solar UV Radiation by H_2O Vapor

Wavelength Range	Reaction	Product Velocities (km sec^{-1})		References	Fraction of Total H_2O Photoabsorbed	
		H Atom	OH Molecule		Quiet Sun	Active Sun
1. 1357Å < λ < 1860Å	$H_2O + h\nu \longrightarrow H + OH(X^2\Pi)$	20	1.2	1, 2, 5, 10	.679	.534
	$\longrightarrow H_2 + O(^1D)$	--	--		.007	.005
2. λ = 1216Å	$H_2O + h\nu \longrightarrow H + OH(X^2\Pi)$	30	1.8	3, 4, 5, 6, 7, 10	.167	.269
	$\longrightarrow H_2 + O(^1D)$	--	--		.023	.036
	$\longrightarrow H + OH^*(A^2\Sigma^+) \longrightarrow H + O + H$	≤ 5.0;?	--		.027	.044
	$\longrightarrow H + OH(A^2\Sigma^+)$	5.0	0.3		.009	.015
3. 984Å < λ < 1357Å, λ ≠ 1216Å	$H_2O + h\nu \longrightarrow H + OH(X^2\Pi)$	25-35	1.2-2.0	3, 4, 5, 6, 7, 10	.028	.021
	$\longrightarrow H_2 + O(^1D)$	--	--		.004	.003
	$\longrightarrow H + OH^*(A^2\Sigma^+) \longrightarrow H + O + H$	4.0-6.0;?	--		.004	.003
	$\longrightarrow H + OH(A^2\Sigma^+)$	0-17.0	0-1.0		.002	.001
4. λ < 984Å	$H_2O + h\nu \longrightarrow$ ionization products [H_2O^+, etc.]	--	--	8, 9	.059	.069

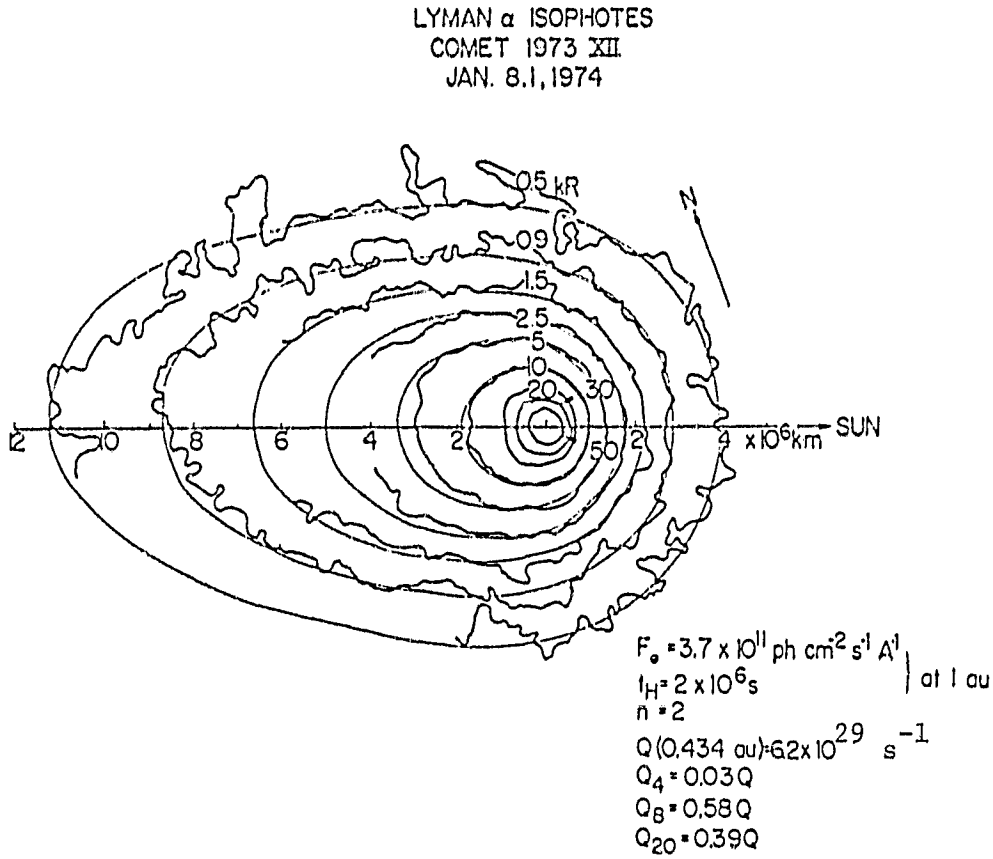

Figure 20. Hydrogen Lyman-α Rocket Image of Comet Kohoutek by Meier et al. (1976). The observed isophotes are shown by the dark contour lines and the model of Meier et al. is shown by the light (smooth) lines. The legend gives numerical parameters for their model.

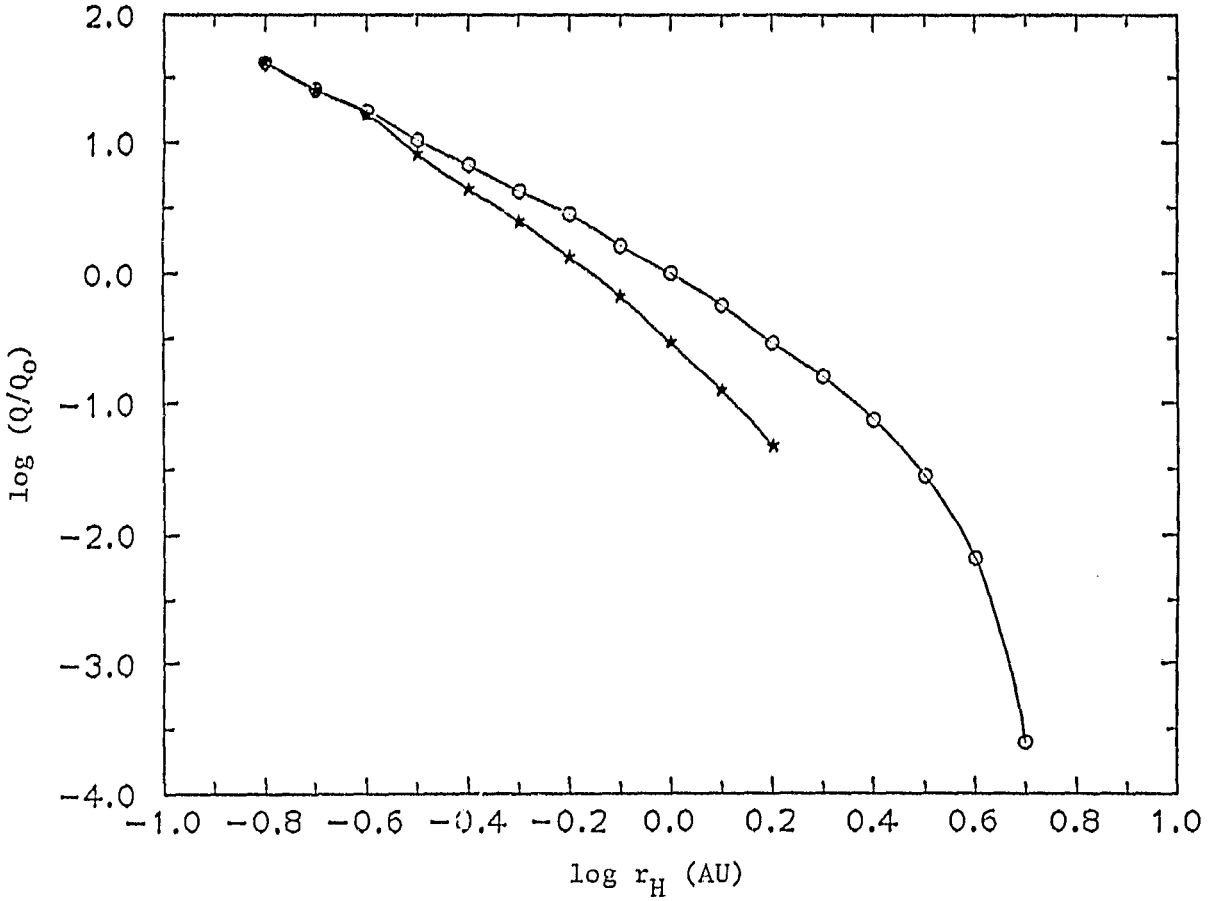

Figure 2[illegible]. Light Curve of Comet Kohoutek 1973XII.
The dependence of the gas production rate for Comet Kohoutek on heliocentric distance has been set in the particle trajectory model from the light curves compiled by Delsemme (1976). The open circles are pre-perihelion points; the stars are post-perihelion. The relative scale has been normalized to the pre-perihelion production rate at 1 AU.

1980). The lifetimes and initial velocities for the various photodissociation products are:

$$\tau_{H_2O} = 8.2 \times 10^4 \; r_H^2 \; s$$

$$\tau_{OH} = 2.0 \times 10^5 \; r_H^2 \; s$$

$$\tau_H = 2.0 \times 10^6 \; r_H^2 \; s$$

$$v_{H_2O} = 0.58 \; r_H^{-0.5} \; km \; s^{-1}$$

$$v_{OH} = 1.2 \; km \; s^{-1}$$

$$v_H = \begin{matrix} 20 \; km \; s^{-1} \\ 8 \; km \; s^{-1} \end{matrix} \qquad \begin{matrix} H_2O + h\nu \rightarrow OH + H \\ OH + h\nu \rightarrow O + H \end{matrix}$$

The modeled Lyman-α image for this case is shown in Figure 22. A comparison of the model with the observation shows that the velocity distribution is still too peaked at 8 and 20 km s^{-1}; the edges of the paraboloid envelopes for the two velocity components are apparent in the model. Thus, a broader velocity distribution, as would be expected if some thermalization of H atoms occurs, is needed.

In order to test this idea, we have introduced two triangular velocity distributions, centered at 8 and 20 km s^{-1} with half-widths equal to the central velocity. The sum of these two distributions reproduces the three Maxwell-Boltzmann distributions of Meier et al. reasonably well. The results of this model are shown in Figure 23. The shape and gradient of the intensity field match the image reasonably well.

The effect of thermalization in particle trajectory models for cometary atmospheres is currently under study in a separate NASA project at AER and will be incorporated into the extended cloud model in the near future. At that point, we will see if a true partially-thermalized distribution can explain the observed Lyman-α image. For the present, we have developed a hydrogen cloud model which can be used to analyze data where collisions are not as important (that is, for the right combination of lower gas production rate and larger heliocentric distance). The model is an improvement over Keller's earlier work in that it includes (1) a spatially extended source

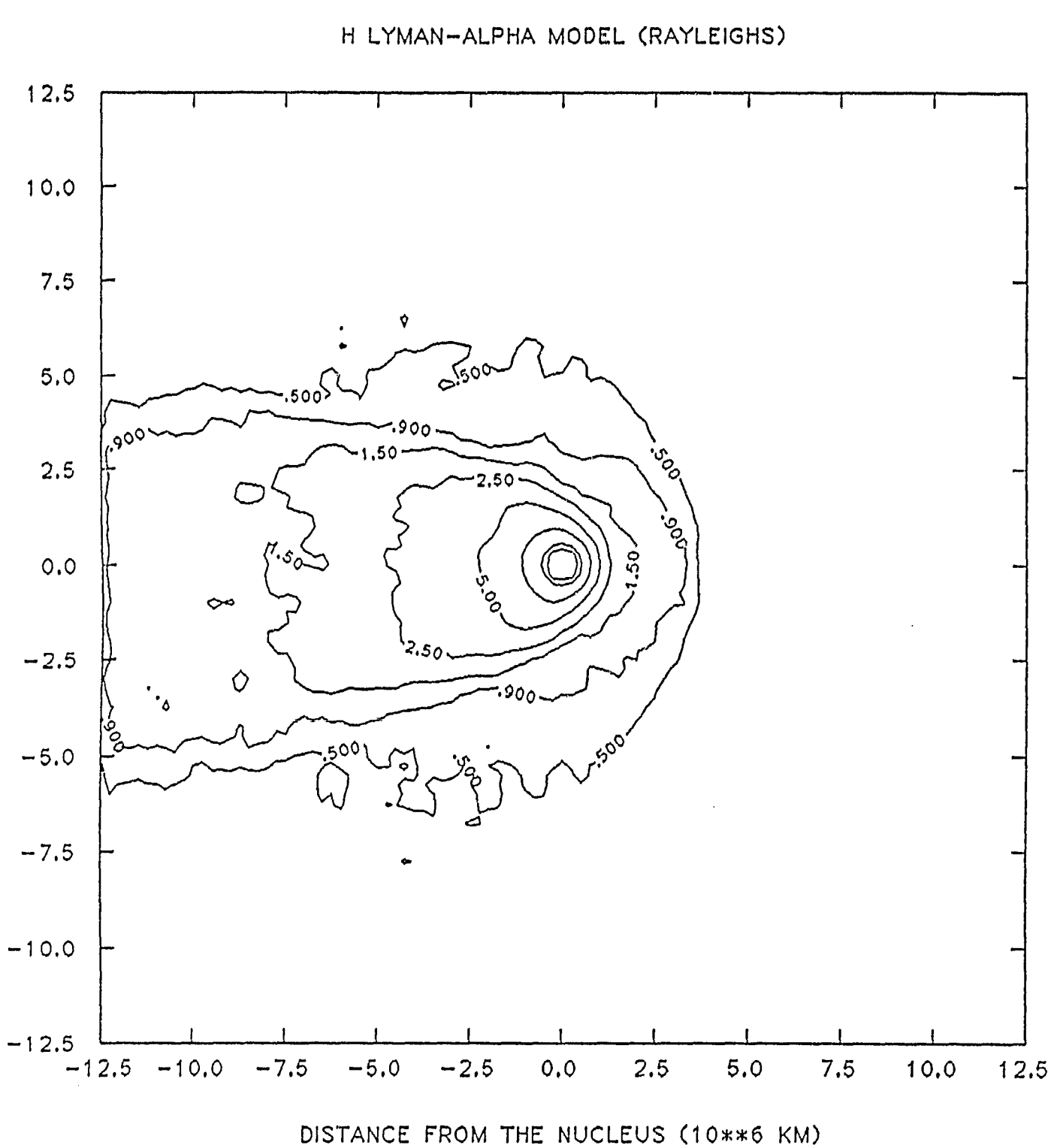

Figure 22. Cometary Hydrogen Particle Trajectory Model: Lyman-α Map for Narrow Peaked Velocity Distribution.

The model run assumed monoenergetic components for hydrogen atoms at 8 and 20 km s^{-1} for photodissociation of OH and H_2O respectively. Contour levels are in kiloRayleights and are the same set as in Figure 20.

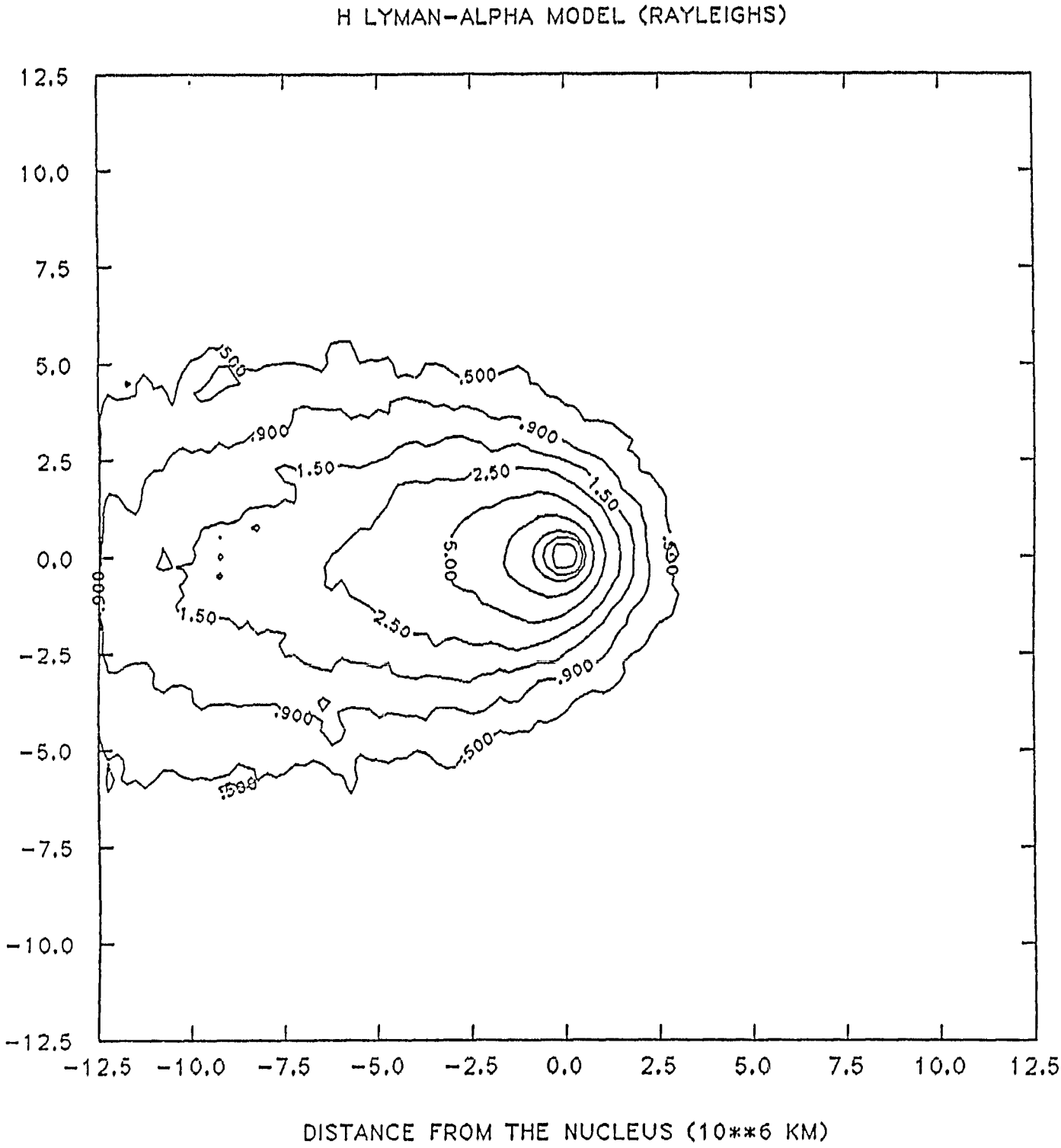

Figure 23. Cometary Hydrogen Particle Trajectory Model: Lyman-α Map for Broadened Velocity Distribution.

The model run assumed triangular velocity distributions centered at 8 and 20 km s^{-1} for photodissociation of OH and H_2O respectively. These two distributions resemble the three Maxwell-Boltzmann distributions used by Meier et al. (1976). Contour levels are in kiloRayleighs and are the same set as in Figure 20.

region, (2) explicit calculation of atom trajectories in three dimensions, and (3) explicit calculation of the time and velocity dependent lifetime, radiation pressure acceleration and excitation rate at each point in the cloud. Keller's models computed these quantities only at the position of the nucleus or at the intersection of a line of sight column with the sky plane.

V. REFERENCES

Acuña, M.H., Behannon, K.W. and Connerney, J.E.P. (1983) Jupiter's Magnetic Field and Magnetosphere. In Physics of the Jovian Magnetosphere, (ed. A.J. Dessler), Cambridge University Press, pp. 1-50.

Bagenal, F. (1984) Plasma Conditions inside Io's Orbit: Voyager Measurements. Preprint.

Bagenal, F., and Sullivan, J.D. (1981) Direct Plasma Measurements in the Io Torus and Inner Magnetosphere of Jupiter. J. Geophys. Res., 86, 8447.

Barbosa, D.D., and Kivelson, M.G. (1983) Dawn-Dusk Electric Field Asymmetry of the Io Plasma Torus. Geophys. Res. Lett., 10, 210.

Bergstralh, J.T., Matson, D.L. and Johnson, T.V. (1975) Sodium D-Line Emission from Io: Synoptic Observations from Table Mountain Observatory. Ap. J., Lett., 195, L131.

Bergstralh, J.T., Young, J.W., Matson, D.L. and Johnson, T.V. (1977) Sodium D-Line Emission from Io: A Second Year of Synoptic Observation from Table Mountain Observatory. Ap. J. Lett., 211, L51.

Bridge, H.S., Sullivan, J.D. and Bagenal, F. (1980) Private communications.

Broadfoot, A. L., et al. (1981) Extreme Ultraviolet Observations from Voyager 1 Encounter with Saturn. Science, 212, 206.

Brown, R.A. and Schneider, N.M. (1981) Sodium Remote from Io. Icarus, 48, 519.

Brown, R.A., Pilcher, C.B. and Strobel, D.F. (1983) Spectrophotometric Studies of the Io Torus. in Physics of the Jovian Magnetosphere, (ed. A.J. Dessler), Cambridge University Press, NY, pp. 197-225.

Combi, M.R. (1980) Neutral Cometary Atmospheres. III. Acceleration of Cometary CN by Solar Radiation Pressure. Ap. J., 241, 830.

Combi, M.R. and Delsemme, A.H. (1980) Neutral Cometary Atmospheres. I. An Average Random Walk Model for Photodissociation in Comets. Ap. J., 237, 641.

Delsemme, A.H. (1976) Physical Interpretation of the Brightness Variation of Comet Kohoutek. In Comet Kohoutek (ed. G. A. Gary). NASA-SP-355.

Delsemme, A.H. (1982) Chemical Composition of Cometary Nuclei. In Comets (ed. Laurel L. Wilkening). The University of Arizona Press, Tucson, Arizona, p. 85.

Festou, M.C. (1981a) The Density Distribution of Neutral Compounds in Cometary Atmospheres. I. Models and Equations. Astron. Astrophys., 95, 69.

Festou, M.C. (1981b) The Density Distribution of Neutral Compounds in Cometary Atmospheres. II. Production Rate and Lifetime of OH Radicals in Comet Kobayashi-Berger-Milon (1975IX). Astron. Astrophys., 96, 52.

Festou, M., Jenkins, G.B., Keller, H.U., Barker, E.S., Bertaux, J.L., Drake, J.F. and Upson, W.L., II (1979) Lyman-Alpha Observations of Comet Kobayashi-Berger-Milon (1975IX) with Copernicus. Ap. J., 232, 318.

Goldberg, B.A. (1983) Private communication.

Goldberg, B.A., Mekler, Yu., Carlson, R.W., Johnson, T.V. and Matson, D.L. (1980) Io's Sodium Emission Cloud and the Voyager 1 Encounter. Icarus, 44, 305.

Hartline, B.K. (1980) Voyager Beguiled by Jovian Carrousel. Science, 208, 384.

Ip, W.-H. and Goertz, C.K. (1983) An Interpretation of the Dawn-Dusk Asymmetry of UV Emission from the Io Plasma Torus. Nature, 302, 232.

Jackson, W.M. (1980) The Lifetime of the OH Radical in Comets at 1 AU. Icarus 41, 147.

Johnson, R.E. (1984) Private communication.

Johnson, R.E. and Strobel, D.F. (1982) Charge Exchange in the Io Torus and Exosphere. J. Geophys. Res., 87, 10385.

Keller, H.U. and Meier, R.R. (1976) A Cometary Hydrogen Model for Arbitrary Observational Geometry. Astron. Astrophys., 52, 273.

Keller, H.U. and Thomas, G.E. (1975) A Cometary Hydrogen Model: Comparison with OGO-5 Measurements of Comet Bennett (1970II). Astron. Astrophys., 39, 7.

Kitamura, Y., Ashihara, O. and Yamamoto, T. (1983) A Model for the Hydrogen Coma of a Comet. ISAS Research Note 153.

Kurucz, R.L. (1983) Private communication.

Lemaire, P., Charra, J., Jouchoux, A., Vidal-Madjar, A., Antzner, G.E., Vidal, J.C., Bonnet, R.M. and Skumanich, A. (1978) Calibrated Full Disk Solar HI Lyman-α and Lyman-β Profiles. Ap. J. Lett. 223, L55.

McFarland, R.H. (1965) Gryziński Electron-Impact Ionization Cross-Section Computations for the Alkali Metals. Phys. Rev., 139, A40.

McFarland, R.H. and Kinney, J.D. (1965) Absolute Cross Sections of Lithium and Other Alkali Metal Atoms for Ionization by Electrons. Phys. Rev., 137, A1058.

Meier, R.R., Opal, C.B., Keller, H.U., Page, T.L., Carruthers, G.R. (1976) Hydrogen Production Rates from Lyman-α Images of Comet Kohoutek (1973XII). Astron. Astrophys., 52, 283.

Münch, G., Trauger, J. and Roesler, F. (1976) Interferometric Studies of the Emissions Associated with Io. Bull. AAS, 8, 468.

Murcray, F.J. (1978) Observations for Io's Sodium Cloud. Ph.D. Thesis, Dept. of Physics, Harvard University.

Pilcher, C.B. (1982) Private communication.

Pilcher, C.B., Smyth, W.H., Combi, M.R. and J.H. Fertel (1984) Io's Sodium Directional Features: Evidence for a Magnetospheric-Wind-Driven Gas Escape Mechanism. To be published in Ap. J., Dec. 1 issue.

Sandel, B.R. and Broadfoot A.L. (1982) Io's Hot Plasma Torus - A Synoptic View from Voyager. J. Geophys. Res. 87, 212.

Schleicher, P.G., and A'Hearn, M.F. (1983) The Photodissociation Lifetime of Cometary OH. Bull. Amer. Astron. Soc. 15, 806.

Schneider, N.M., Hunten, D.M. and Brown, R.A. (1984) New Evidence for High-Density Inclusions in the Io Plasma Torus. Bull. AAS 16, 663.

Scudder, J.D., Sittler, E.C., Jr. and Bridge, H.S. (1981) A Survey of the Plasma Electron Environment of Jupiter: A View from Voyager. J. Geophys. Res., 86, 8157.

Shemansky, D.E. (1980) Private communication.

Shemansky,D. E. (1984) Private communication.

Shemansky, D.E. and Sandel, B.R. (1982) The Injection of Energy into the Io Plasma Torus. J. Geophys. Res. 87, 219.

Shemansky, D. E. and Smith, G.R. (1982) Whence Comes the "Titan" Hydrogen Torus? EOS, 63, 1019.

Shemansky, D.E., Smith, G.R., Smyth, W.H. and Combi, M.R. (1984) The Distribution of Atomic Hydrogen in Saturn's Magnetosphere. Bull. AAS 16, 712.

Sieveka, E.M. and Johnson, R.E. (1984) Ejection of Atoms and Molecules from Io by Plasma-Ion Impact. To appear in Ap. J., Dec. 1 issue.

Sittler, E.C. (1984) Private communication.

Smyth, W.H. (1981) Titan's Hydrogen Torus. Ap. J., 246, 344.

Smyth, W.H. (1983) Io's Sodium Cloud: Explanation of the East-West Asymmetries. II. Ap. J., 264, 708.

Trafton, L. (1975) Detection of a Potassium Cloud near Io. Nature, 258, 690.

Trafton, L. (1977) Periodic Variations in Io's Sodium and Potassium Clouds. Ap. J., 215, 960.

Trafton, L. (1981) A Survey of Io's Potassium Cloud. Ap. J., 247, 1125.

Trauger, J.T. (1984) Photometric Images of Sulfur Ions and Sodium Neutrals in the Jupiter/Io Torus. Bull AAS 16, 712.

Trauger, J., Roesler, F. and Münch, G. (1976) Velocity Scructure in the Sodium Emission from Io. Bull. AAS, 8, 468.

van Dishoeck, E.F. and Dalgarno, A. (1984) The Dissociation of OH and OD in Comets by Solar Radiation. Icarus 59, 305.

Whipple, F.L. (1980) Rotation and Outbursts of Comet P/Schwassmann-Wachmann 1. Astron. J. 85, 305.

Zapesochnyi, I.P. and Aleksakhin, I.S. (1968) Ionization of Alkali Metal Atoms by Slow Electrons. Zh. Eksp. Teor. Fiz., 55, 76. [Also, Soviet Physics, JETP 28, 41 (1969).]

VI. REFERENCES FOR TABLE 4

1. Stief, L.J., Payne, W.A. and Klemm, R.B. (1975) J. Chem. Phys. 36, 605.

2. Welge, K.H. and Stuhl, F. (1967) J Chem. Phys. 16, 2440.

3. Carrington, T. (1964) J. Chem. Phys. 41, 2012.

4. McNesby, J.R., Tanaka, I., and Okabe, H. (1962) J. Chem. Phys. 36, 605.

5. Festou, M.C. (1981) Astron. Astrophys. 96, 52.

6. Slanger, T.G. (1982) Private communications.

7. Lee, L.C. (1980) J. Chem. Phys. 72, 4334.

8. Oppenheimer, M. and Downey, C.J. (1980) Ap. J. Lett. 241, L123.

9. Hudson, R.D. (1971) Critical review of UV photoabsorption cross sections for molecules of astrophysical and aeronomic interest. Natl. Stand. Ref. Data Ser., Natl. Bur. Stand. (U.S.) 38, 50-52.

10. Okabe, H. (1978) Photochemistry of Small Molecules. John Wiley & Sons, Inc., New York, pp. 201-203.